Chapter 3
Atmospheric Electricity

Abstract In this chapter the main attention is paid on the atmospheric electricity and on the global lightning activity as a machine supplying the negative charges to the Earth. Here we deal with the electric field and charge distribution in thunderstorm clouds and with the conventional mechanism for air breakdown. Lightning discharge parameters and global thunderstorm activity are discussed. In the remainder of this chapter the main emphasis is on the low frequency effects associated with recently documented evidences of previously unknown forms of upward propagating gigantic electric discharges, also known as transient luminous events (TLEs), which occur above a large thunderstorm system.

Keywords Global thunderstorm activity • Lightning return stroke • Runaway electron breakdown • Streamer • Transient luminous events (TLEs)

3.1 Global Electric Circuit

3.1.1 Electric Field and Conductivity of the Atmosphere

It is usually the case that the clouds, precipitation, fogs, and dust clouds contain a large amount of spatial electric charges. The electric field permanently exists in the atmosphere even though there is a fine weather condition. Near the ground surface the so-called fair weather electric field, i.e., the steady electric field, is vertically downward with mean value of about 100–130 V/m. The solid Earth is negatively charged with net charge about -3×10^5 C, while the positive charges are mainly concentrated in the lower atmosphere. Under fair weather conditions the atmospheric electric field falls off with height as shown in Fig. 3.1, so that its value is no more than several volts per meter at the height about 10 km. Owing to the presence of charged aerosols the electric field may increase in amplitude in the mixing layer over

Fig. 3.1 Typical profile of
the electric field in the
atmosphere. *1*—fair weather
conditions over ocean, arctic
region and etc. *2*—over
mainland. Adapted from the
site http://www.femto.com.
ua/articles/part_1/0217.html
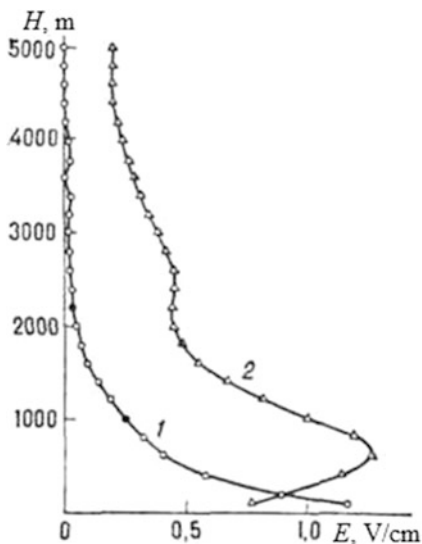
the land, as shown in Fig. 3.1 with line 2. Above the mixing layer, whose depth is
about 0.3–3 km, the field value decreases approximately exponentially. The voltage
drop between the Earth and the ionosphere is about 200–250 kV.

The atmospheric conductivity at the ground level is about $\sigma_a = (2-3) \times 10^{-14}$ S/m which is smaller than that of the ionosphere by several orders of
magnitude. In the mixing layer the atmospheric conductivity σ_a increases insignifi-
cantly and then it rises nearly exponentially with altitude, with a characteristic scale
of 3–7 km, the value of which depends on altitude. For example, at the daytime
conditions the approximate law for the conductivity as a function of altitude z can
be written as (Chalmers 1967)

$$\sigma_a = \sigma_0 \exp\left(z/z_0\right), \quad 0 < z < 3.6\,\text{km},$$
$$\sigma_a = \sigma_1 \exp\left(z/z_1\right), \quad 3.6 < z < 17.7\,\text{km},$$
$$\sigma_a = \sigma_2 \exp\left(z/z_2\right), \quad 17.7 < z < 40\,\text{km}, \tag{3.1}$$

where $z_0 = 0.82$ km, $z_1 = 4.1$ km, $z_2 = 7.0$ km, $\sigma_0 = 1.14 \times 10^{-14}$ S/m, $\sigma_1 = 0.38 \times 10^{-12}$ S/m, and $\sigma_2 = 2.29 \times 10^{-12}$ S/m. This exponential tendency holds true
for larger altitudes although the atmospheric conductivity depends on local time.

Above the lower edge of the E region at altitudes 75–90 km the ratio of the
electron gyrofrequency to the electron–neutral collision frequency is no longer
negligible, and the conductivity converts from a scalar quantity to a tensor one.
Note that the atmospheric conductivity undergoes diurnal variations depending on
latitude, local meteorological conditions, and so on.

The so-called fair weather current, that is, a weak background current flowing
from the mesosphere to the ground plays an important role in the generation of

global electric circuit. The mean value of the background atmospheric current density is about $(3.5–4) \times 10^{-12}$ A/m^2 (e.g., see Feynman et al. 1964). In stratus rainclouds the vertical atmospheric current increases up to $(0.5–1) \times 10^{-11}$ A/m^2, and in storm precipitation it enhances up to $10^{-10}–10^{-9}$ A/m^2.

This current is mostly due to the atmospheric conductivity although the diffusion and convective transfer of the electric charges may also be operative in the atmosphere. The convection and diffusion currents may be comparable to the conduction current within the mixing layer, whereas the sum of these currents is approximately the same as the conduction current at high altitude since the net current usually exhibits weak variations with altitude. In contrast to that the conductivity and electric field can be highly dependent on altitude. As an example, it is worthwhile to mention the case of mesospheric altitudes in which layered peaks of downward electric field and relatively low conductivity have been occasionally detected (Bragin et al. 1974; Hale et al. 1981; Maynard et al. 1981).

The permanent thunderstorm activity around the world is thought to be a major electric source for the global atmospheric electric circuit, which is formed by the lower ionosphere and terrestrial surface conducting layers (e.g., see Rakov and Uman 1998, 2003). The global electric circuit is closed via lightning discharge currents flowing basically upwards and the background atmospheric current flowing downward to the Earth's surface from the atmosphere and lower ionosphere. A typical negative cloud-to-ground (−CG) lightning flash carries about $q = -20$ C of the negative electricity. Taking into account that worldwide number of the lightning discharges per second is about $\nu = 10^2$ s^{-1} we obtain that the total current flowing to the Earth is $I = |q| \nu \approx 2 \times 10^3$ A. Based on Optical Transient Detector (OTD) satellite data one can specify this value since the global annual mean flash frequency has recently been estimated as 44 ± 5 s^{-1} (Nickolaenko and Hayakawa 2002, 2014; Christian et al. 2003; Hayakawa et al. 2005; Sato et al. 2008; Sátori et al. 2009).

The negative sign of the typical lightning charge means that the flash current points outward, that is, from the Earth to the ionosphere. The opposite-directed conduction current carries the positive charges from the upper atmosphere and troposphere to the Earth. Assuming for the moment that this background conduction current is approximately uniformly distributed around the Earth, the total current flowing from the ionosphere to the Earth surface can be estimated as $I_f = 4\pi j_f R_e^2$, where j_f is the mean density of the background current and R_e is Earth radius. Taking the numerical values of the parameters $j_f \approx (3–4) \times 10^{-12}$ A/m^2 and $R_e \approx 6.4 \times 10^3$ km we get the estimate $I_f \approx (1.5–2) \times 10^3$ A, which is consistent in magnitude with the inverse background current due to the global thunderstorm activity.

3.1.2 Electric Field and Charges in Thunderstorm Clouds

At the moment there are about 2,000 thunderstorms simultaneously operating on the Earth. As the global mean flash frequency is about 10^2 s^{-1}, the individual
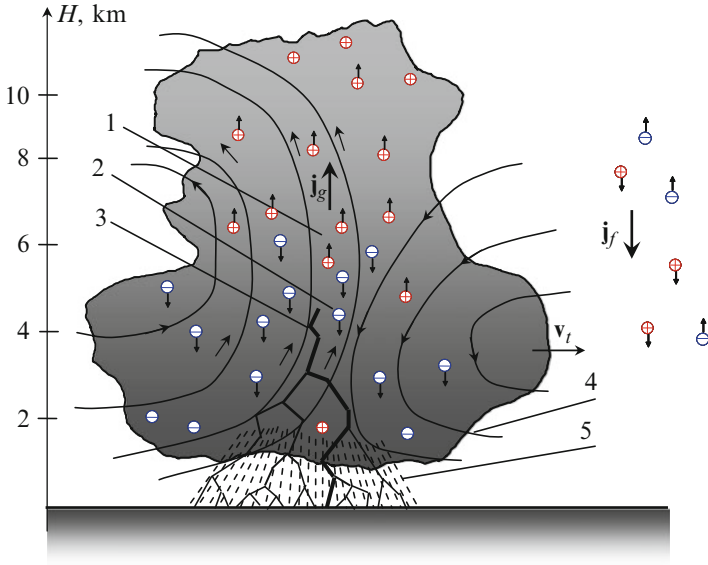
Fig. 3.2 A sketch of thundercloud structure. *1* and *2*—centers of positive and negative charge distributions. *3*—a lightning return stroke. *4*—air flow lines. *5*—a downpour. *Horizontal arrow* $\mathbf{v}_t$ shows the direction of the thundercloud motion

thunderstorm is characterized by the local mean flash frequency about $0.05\,\mathrm{s}^{-1}$. Whence we can estimate the mean interval between lightning flashes as 20 s. The charge of thunderstorm clouds is thus renewed for this short interval of time.

We now raise an interesting question, what is the basic mechanism for electric charge formation in the thunderstorm cloud? The electric charges in the clouds are concentrated on the small particles such as rain-drops, snowflake, pieces of ice and aerosols. In stratus and stratocumulus clouds the charge of rain-drop reaches the value of $q_0 = (10$–$100)\,e$, where e is elementary charge, while in the nimbostratus the charges of separate drops amounts to $q_0 = \left(10^5$–$10^6\right) e$ and in the thunderstorm clouds the separate charges amounts to a very great value of the order of $\left(10^6$–$10^7\right) e$ (Israël 1970, 1973, Imyanitov et al. 1971, Muchnik and Fishman 1982).

Despite that the electrical structure of a typical thundercloud is rather a stratiform, the most part of positive charges tend to pile up at the upper portion of the thundercloud whereas most of negative charges predominantly accumulate at its bottom (Coroniti 1965; Nelson 1967; Bhartendu 1969; Wahlin 1973; Winn et al. 1974; Uman 1987; McGorman and Rust 1998; Rakov and Uman 2003). The simplest model of the spatial charge separation in the thundercloud is shown in Fig. 3.2. In the middle latitudes the thundercloud top amounts to 8–12 km, while in tropics the thundercloud top may be as high as 20 km. The thunderstorms are mainly formed in the zone of power convective fluxes. The separation of oppositely

Fig. 3.3 A simplified model of electric charge distribution in a thundercloud. The spatial charge densities are constant inside the spherical regions whose centers are located on the z-axis at different altitudes and z_1, z_2, z_3, and z_4 (Surkov and Hayakawa 2012)
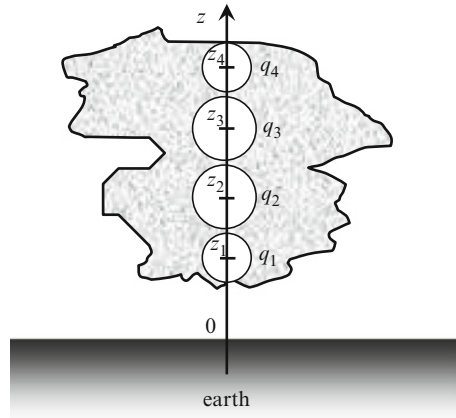
charged particles is thought to be due to slow hydrodynamics processes inside the thundercloud. It appears that upward air fluxes drag small and light positively charged ice fragments, whereas heavy negatively charged hailstones predominantly fall downward due to the gravity (Lyons et al. 2003; Lyons 2006; Krehbiel et al. 2008; Pasko 2010). Since the current is upward inside the thundercloud and approximately zero outside, charges pile up at the thundercloud boundaries as shown in Fig. 3.2. Here $\mathbf{j}_g$ is updrafts- and gravity-driven current density inside the thundercloud. This current causes the charge separation in the thundercloud and thus it plays a role of a battery/source for the generation of upward or downward-directed lightning discharges. $\mathbf{j}_f$ denotes the so-called fair weather current. The lightning can be operative as long as the current $\mathbf{j}_g$ can separate the charges and provide the top of the thundercloud with sufficient amount of positive charges.

The charge density, ρ, which is usually observed under the fine weather condition is about $0.01 \, \text{nC/m}^3$. In stratocumulus clouds the charge density increases up to $0.1 \, \text{nC/m}^3$. In cumulonimbus clouds under the downpour the mean charge density is about $\rho = 0.3$–$10 \, \text{nC/m}^3$ while in the thunderclouds $\rho = 3$–$30 \, \text{nC/m}^3$ (Imyanitov et al. 1971).

Notice that the electrical structure/charge distribution of actual thunderclouds is much more complicated as compared to the above model. Moreover a certain charge imbalance may persist in a thunderstorm, which leads to strong variations of the electric field with altitude. The electrical structure of a standard thundercloud can be described via a stratiform/multilayered thundercloud model in which the charged regions are situated at different altitudes (Krehbiel et al. 2008; Riousset et al. 2010a). The spatial distribution of these charges was assumed to obey a Gaussian law and was not spherically symmetric. To simplify the problem and to interpret this model, we assume that all the charges are uniformly distributed in spherical regions shown in Fig. 3.3. A normally electrified storm, which corresponds to a typical $-CG$ lightning, was characterized by the following numerical values $q_i = 12.5, -60, 40$, and $-20 \, \text{C}$, where $i = 1, 2, 3, 4$ (Krehbiel et al. 2008). The Earth is considered to

be a perfect conductor. This implies that the vertical component of the net electric field taken along the z-axis is given by $E_z = \sum\limits_{i=1}^{4} E_{zi}$, where

$$E_{zi} = \frac{q_i (z - z_i)}{4\pi \varepsilon_0 r_i^3} + E_{zi}' \tag{3.2}$$

inside the charged balls and

$$E_{zi} = \frac{q_i (z - z_i)}{4\pi \varepsilon_0 |z - z_i|^3} + E_{zi}' \tag{3.3}$$

outside the balls. Here

$$E_{zi}' = \frac{q_i}{4\pi \varepsilon_0 (z + z_i)^2} \tag{3.4}$$

stands for the electric field of mirror electric images of thundercloud charges, and z_i denote the coordinates of centers and radii of the charged spherical regions, respectively. The variations of the net electric field, E_z, as a function of altitude z can be easily calculated after these simplifications.

To illustrate the results of this simulation we made use of the following numerical parameters $z_i = 3.7, 6.9, 12.1, 15.7$ km, $r_i = 1.0, 2.2, 2.3, 1.3$ km and above-mentioned values of q_i taken from Krehbiel et al. (2008). The results of calculations shown in Fig. 3.4 with solid line are in qualitative agreement with the vertical profiles of thunderstorm electric field as measured by balloon equipment (Marshall et al. 1995). The first two peaks at the bottom of Fig. 3.4 are basically due to the field of a pair of charges $q_1 = 12.5$ C and $q_2 = -60$ C whereas the two peaks at the top of Fig. 3.4 are caused by the upper charges $q_3 = 40$ C and $q_4 = -20$ C. It should be noted that both the magnitude and location of the peaks are very sensitive to the distances between the charges.

3.1.3 Conventional Mechanism for Air Breakdown and Streamers

The conventional mechanism of air breakdown is due to the thermal ionization of the air by low energy electrons in the presence of strong electric fields, which occasionally occurs inside and around thunderclouds. Typical energy of electrons producing the ionization is about 10–20 eV while the mean electron energy is about 2 eV. According to laboratory tests the breakdown threshold E_c is approximately proportional to the gas pressure p at least under condition $pd > 10^6$ Pa m, where d is the inter-electrode gap size (e.g., see Raizer 1991; Lieberman and Lichtenberg 1994). It follows from the state equation of perfect gas ($p = k_B n_m T$) that at constant
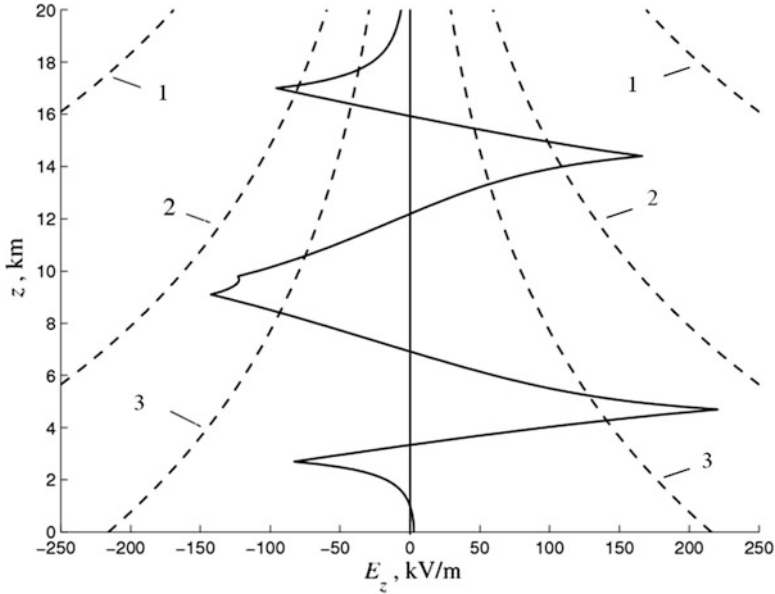
Fig. 3.4 Model calculations of thunderstorm quasielectrostatic (QE) field preceding a conventional −CG stroke. The vertical electrical field profile along *z*-axis as a function of altitude *z* is shown with solid line. The fields required for the propagation of negative and positive streamers in the air are shown with *dash lines* 1 and 2, respectively. A runaway breakdown field is shown with *dash line* 3. The numerical values of parameters are assumed to be typical for the generation of −CG strokes (Surkov and Hayakawa 2012)

gas temperature the value of E_c is proportional to number density n_m of the neutral gas. Taking into account of Eq. (2.3) for n_m we thus obtain that the conventional breakdown threshold falls off approximately exponentially with altitude

$$E_c = E_0 \exp\left(-z/H_a\right). \tag{3.5}$$

Here $E_0 \approx 32 \, \text{kV/m}$ is the constant of the order of breakdown threshold at the ground level.

As the electric field exceeds the breakdown threshold (3.5), the streamer mechanism of air breakdown may develop (e.g., see Bazelyan and Raizer 1998). A typical streamer is the self-propagating narrow filament of cold low-conducting plasma which can propagate at the velocity 10^2–$10^4 \, \text{km/s}$ as measured at the ground pressure. The electric field in the vicinity of the streamer head can be about 4–7 times larger than E_c due to the high charge density at streamer head. This results in the electron impact- and photo-ionization in the streamer head followed by an enhancement of ionization coefficient up to the value occurring at the streamer channel (e.g., Raizer et al. 1998; Pasko 2006; Celestin and Pasko 2010). In laboratory experiments such as point-to-plane corona discharges, the individual electron avalanches initiate the streamer in the vicinity of the sharp portion of an

electrode thereby producing the streamer branching phenomena. The transition from an electron avalanche to a streamer generation also requires the critical number of avalanching electrons, a minimum radius of the avalanche region and many other factors (e.g., Raizer et al. 1998; Bazelyan and Raizer 1998).

The streamers can be divided into two types depending on the sign of the space charge in their heads. A negative streamer propagates due to ejection of electrons from its head into ambient air and vice versa, that is a positive streamer propagates due to injections of ambient/seed electron avalanches from surroundings. Along with the traditional channels of the seed electron production such as the cosmic rays and photo-ionization of air due to solar radiation, the effective source of the electron production is the strong electric field at the streamer head which gives rise to the high rate of impact- and photoionization around the head (Bazelyan and Raizer 1998). In electronegative gases such as air, the oxygen and nitrogen ions could be an additional source of seed electrons due to fast electron detachment in an electric field (Pancheshnyi 2005).

In some sense, the streamers can be considered as a kind of ionization waves which require the strong electric field for their initiation. However, once the steamer was generated it can propagate through the region where the electric field is smaller than E_c. The minimum value of electric field required for the propagation of positive streamers in the air at ground pressure is $E_s^+ = 4.4\,\text{kV/cm}$, while the same value for negative streamers is $E_s^- = -12.5\,\text{kV/cm}$ (Raizer 1991; Allen and Ghaffar 1995; Babaeva and Naidis 1997; Pasko 2006). The dependence of these values on altitude is described by an equation analogous to Eq. (3.5). The altitude-dependences of electrical field required for breakdown in the air are shown in Fig. 3.4 with lines 1–3, which correspond to different mechanisms of the air breakdown. We shall discuss the runaway breakdown mechanisms (line 3) in more detail later on. Despite the calculated value of electric field does not exceed the breakdown threshold for streamer propagation, the lightning nucleation is the most probable in the regions where the peaks of thunderstorm electric field are close to the breakdown threshold. Random spatial inhomogeneities of the charge distribution may increase the local electric field. As is seen from Fig. 3.4, the lightning discharge between the cloud and ground may be initiated in the vicinity of the first peak at 4–6 km altitude range.

3.1.4 Lightning Discharge

The first studies have shown that the streak lightning originated from the thundercloud is a sort of spark discharge with length of several kilometers and with peak current of about 20 kA (e.g., see Stekolnikov 1940; Schonland 1956; Ishikawa 1961). The typical lightnings can be divided into two general classes: cloud-to-ground (CG) and intracloud (IC) lightning discharges. A newly discovered class of high-altitude gigantic discharges occurring above a large thunderstorm
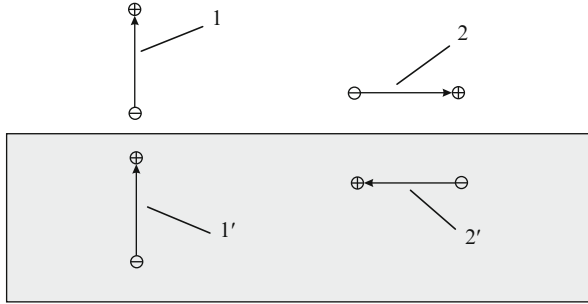
Fig. 3.5 Vertical and horizontal dipoles above the perfect conducting ground. The vertical dipole is approximately duplicated due to the electric images in the ground while the horizontal dipole is converted to quadrupole

at stratospheric and mesospheric altitudes (Franz et al. 1990) is discussed in the Sect. 1.3.2. The IC discharges are strongly prevalent over the CG and transient luminous events (TLEs). Note that the peak current of the IC discharges is one order of magnitude smaller than that for CG discharges. However the IC discharges may have a length up to 50–150 km.

Effectiveness of the vertical and horizontal discharges, considered as electromagnetic wave transmitter, is extremely different (Kudintseva et al. 2009; Hayakawa et al. 2012). To illustrate this, we approximate the actual discharge with the effective electric dipole/antenna shown in Fig. 3.5 with lines 1 (CG) and 2 (IC). If the ground is considered as a perfect conductor, the electric field of induction electric charges arising on the ground surface is equivalent to the electric field of dipole image, which is in the ground symmetrically with respect to the ground surface as shown in Fig. 3.5 with lines 1′ and 2′. In the vertical case it practically produces the duplication of the net dipole moment, whereas in the horizontal case the net dipole moment vanishes, so that the horizontal antenna is equivalent to a quadrupole. This implies that CG lightning can be a much stronger radiator as compared to IC especially in ULF/ELF (extremely low frequency, < 3 kHz) range. One more argument in favor of this statement is the presence of the so-called continuing current (CC) following the CG flash because the CC may greatly contribute to the ULF/ELF portion of the lightning spectrum. The IC lightning cannot, in general, be observed at distances as great as CG lightning (Heavner et al. 2003). The energetic intracloud (EIC) discharges are the most powerful source of lightning radiation in the HF (high frequency) and VHF (very high frequency) radio bands (e.g., see Smith et al. 1999, 2004; Jacobson 2003). Certainly the portion of the EIC with vertical channels may also contribute to the background ULF/ELF electromagnetic noise produced by the global lightning activity. However in what follows the main emphasis is on the CG lightning as the most creditable candidate for the excitation of global electromagnetic low-frequency resonances.

To a great extent our knowledge of the lightning parameters comes from the optical and electromagnetic measurements in the VLF (very low frequency) and other regions (e.g., see Uman 1987; Raizer 1991; Nickolaenko and Hayakawa 2002, 2014; Rakov and Uman 2003). As noted above, the majority of CG lightning are negative. This implies that the current of the lightning discharge is upward-directed which corresponds to the positive current moment. The −CG lightning discharge starts with the downward-propagating stepped leader, which creates the thin conducting plasma channel that connects the thundercloud to the ground. The leader motion can be divided into two phases. At the first phase the pilot-streamer, which arises in the thundercloud, begins to move jerkily. On the average, during the jerk the streamer travels a distance about 100 m at the mean velocity of the order of 5×10^2 km/s. Then the heavily ionized leader catches up with the streamer front for a short time of about 1 μs. The leader velocity is believed to be about 7×10^4 km/s. After that a new pilot-streamer arises from the end of the ionized channel and a newly leader catches up with the streamer front and etc. step-by-step, so that the ionized channel makes longer. The mean pause between the leader steps is about 50 μs. It is usually the case that the channel branches out when it moves downward to the ground. The stepped leader carries the negative charge of the order of 5 C with the mean vertical velocity of 1.5×10^2 km/s and the leader current is as high as 300 A.

The subsequent upward-propagating return stroke produces a main breakdown of the CG interval. The return stroke is an upgoing wave propagating rapidly along the warm conducting channel. The stroke begins to move with the velocity $(0.5–1) \times 10^5$ km/s and further it decelerates gradually. During an interval of 5–10 μs the return stroke current amounts to the peak value 10–20 kA and thereafter the current decreases up to half the peak value for the interval about 20–50 μs. The net result of a leader/return-stroke pair is that negative charge of about 10 C is lowered from the thundercloud to the ground.

The −CG lightning flash usually contains return strokes and the mean interval between the strokes is 40 ms, so that the net duration of the flash is about 0.2 s. Note that leaders preceding the second and subsequent strokes propagate continuously without any steps and pauses. Such leaders termed as dart leaders move at the velocity 10^3–10^4 km/s that is much higher than that of the stepped leader. A highly branched system of the streamer channels arises around the leader (Uman 1987; Rakov and Uman 2003).

A portion of −CG return strokes is accompanied by the CC that immediately follows the return strokes. This current of several tens to hundreds of amperes flows in the same channel to the ground for tens to hundreds of milliseconds (e.g., see Rakov and Uman 2003). Thus the CC manifests itself as a slowly varying current flowing between the thundercloud and ground along the path created by the preceding leader return stroke pairs. This current makes a significant contribution to the low-frequency portion of natural electromagnetic noise especially to ULF/ELF region which contains global electromagnetic resonances (see Chap. 2).
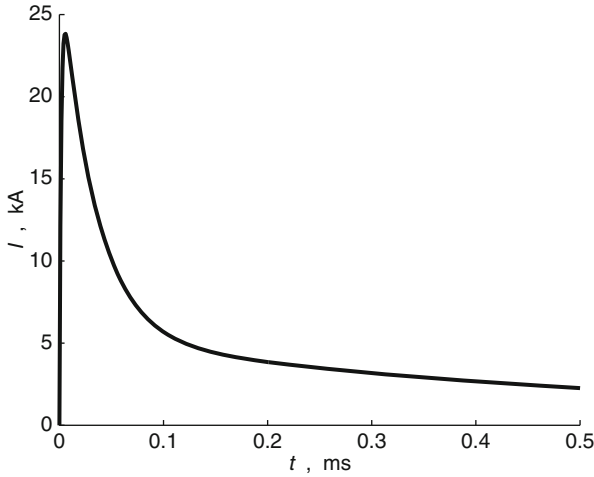
**Fig. 3.6** Model calculation of the return stroke current versus time

It is thought that about 5–10 % of global CG lightning activity is composed of positive cloud-to-ground (+CG) lightning, which transfers the positive charge to the ground (Rakov 2003). A positive flash usually consists of a single stroke followed by a CC that typically lasts for several tens or hundreds ms. The amplitude of positive CC current varies from several kA to tens kA, an order of magnitude larger than that for the −CG (Rakov 2003; Rakov and Uman 2003). The reader is referred to the extensive special literature for details about CG and IC lightning discharges (e.g., see Krider 1986; Uman 1987; Raizer 1991; Lyons 1997; McGorman and Rust 1998; Rakov and Uman 2003 and references therein).

There are a number of relevant models, which can serve as "engineering" models of lightning stroke (Rakov and Uman 1998). According to the known models for a −CG lightning, the current at the base of the stroke is described by a combination of a power function and several exponents with different relaxation times (e.g., see Nickolaenko and Hayakawa 2002). More usually we choose four items in this model (e.g., see Jones 1970; Taylor 1972; Uman and Krider 1982; Uman 1987)

$$I(t) = \sum_{m=1}^{4} I_m \exp(-\omega_m t) \tag{3.6}$$

where ω_m are inverse time constants. Since the current given by Eq. (3.6) is equal to zero at the initial moment $t = 0$, the amplitudes I_m of individual current terms must satisfy the condition $\sum_{m=1}^{4} I_m = 0$. Following Jones (1970) we use the following values of the parameters, which are typical for the models of return strokes $I_{1-4} = -28.45, 23.0, 5.0, 0.45$ (in kA) and $\omega_{1-4} = 6.0 \times 10^5, 3.0 \times 10^4, 2.0 \times 10^3, 147.0$ (in s^{-1}). Figure 3.6 shows the temporal variation of the return stroke current for these parameters.

Fig. 3.7 Model calculation of current moment of a return stroke versus time
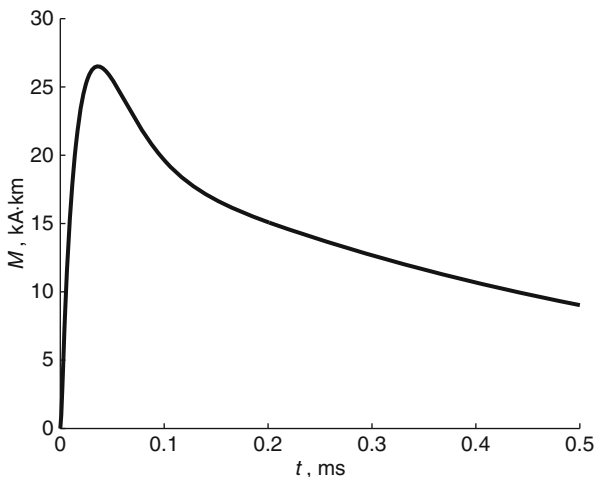
The two last terms on the right-hand side of Eq. (3.6), that is $I_3 \exp(-\omega_3 t) + I_4 \exp(-\omega_4 t)$, describe the CC, which is responsible for the final decay of the electrostatic field of the stroke. As we have noted above, a $-$CG stroke transfers the negative electric charge to the ground and the lightning current is thus pointed upward. It follows from the model that the total lightning charge equals -6.3 C, and about 50% of this charge is carried by the weak CC, which is described by the component I_4 and, in part, by the component I_3. Below we show that these terms make a main contribution to the ULF range of the lightning spectrum.

Far from the lightning discharge the ULF electromagnetic field can be characterized by the current moment of the stroke as the product of the discharge current and the length of the current channel, i.e., $m(t) = I(t)\, l(t)$. One more important lightning characteristic is the charge moment, which is equal to the product of the total charge transferred from the thundercloud to the ground and the final length of the current channel.

In the theory the lightning channel length, l, is assumed to be governed by an exponential law $dl/dt = V_0 \exp(-\Omega t)$, where V_0 is the current wave velocity at the ground level (see Ogawa 1995). In another words, the vertical current channel grows upward with exponentially attenuated velocity. In this case

$$m(t) = M F_1(t)$$
$$F_1(t) = [1 - \exp(-\Omega t)] \sum_{m=1}^{4} \frac{I_m}{|I_1|} \exp(-\omega_m t) \tag{3.7}$$

where $M = |I_1|\, l$ and $l = V_0/\Omega$ is the final channel length.

For illustrative purposes, a model calculation of the lightning current moment is shown in Fig. 3.7 as a function of time. In making the plot of $m(t)$ we have used the following numerical values of parameters: the maximum of lightning channel velocity is $V_0 = 8 \times 10^4$ km/s and the inverse time parameter is $\Omega = 2 \times 10^4$ s^{-1}.
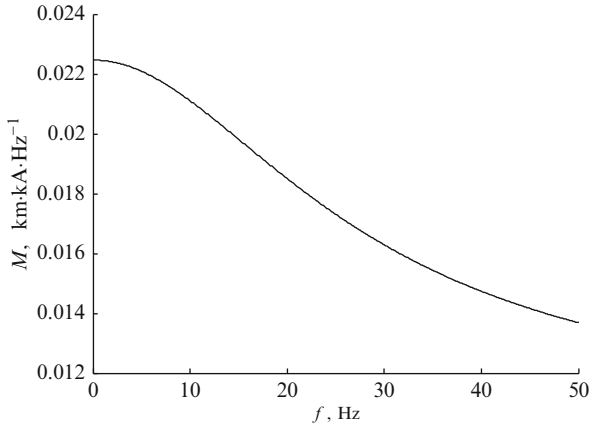
Fig. 3.8 Model calculation of the absolute value of current moment spectrum of an individual return stroke

Whence it follows that the final channel length is $l = V_0/\Omega = 4\,\text{km}$ (see, e.g., Berger et al. 1975; Nickolaenko and Hayakawa 1998, 1999, 2002; Visacro et al. 2004). As is seen from Fig. 3.7, the current moment magnitude is about $27\,\text{kA}\,\text{km}$ for these parameters.

The spectrum of the current moment $M(t)$ can be written as

$$m(\omega) = M F_1(\omega) = V_0 \sum_{m=1}^{4} \frac{I_m}{(\omega_m - i\omega)(\omega_m + \Omega - i\omega)} \qquad (3.8)$$

As illustrated in Fig. 3.8 the absolute value of the return stroke spectrum by Eq. (3.8) is practically constant within the ULF band. It is not surprising since in this case $\omega \ll \omega_m$ and thus the frequency-dependent terms in the denominator of Eq. (3.8) are negligible.

3.1.5 Multiple Return Stroke

As we have noted above, a typical $-$CG lightning discharge consists of $n = 2 - 6$ return strokes. More frequently there are 3–4 return strokes with characteristic duration of about $100\,\mu\text{s}$ (Uman 1987; Ogawa 1995; Lyons 1997; McGorman and Rust 1998; Borovsky 1998). The mean interval between them is of the order of $t_0 = 40\,\text{ms}$. The current profile of the individual strokes can be different.

Now we consider a simple model of multiple return stroke proposed by Jones (1970). The final/peak length of each return stroke is assumed to increase with its

number n by the fixed value Δl, that is, as $l_n = l_1 + (n-1)\,\Delta l$. The increase in the lightning channel length results in gradual enhancement of the electric current moment.

Actually the current profiles of the individual strokes can be different whereas in this model all the current impulses are assumed to have the same shape. The inverse time parameter, Ω_n, of the return stroke is related to the channel length, l_n, as follows

$$\Omega_n^{-1} = \frac{l_n}{V_0} = \Omega_1^{-1} + \frac{\Delta l}{V_0}\,(n-1)\,, \tag{3.9}$$

where $\Omega_1 = V_0/l_1$. The net magnetic moment of the flash which contains the multiple discharge can be described by an equation analogous to Eq. (3.7), that is $m(t) = MF(t)$, where $M = l_1\,|I_1|$ is the "magnitude" of the current moment while the dimensionless function $F(t)$ determines the shape of the multiple discharge

$$F(t) = \sum_{n=1}^{n_0} \frac{l_n}{l_1} \left[1 - \exp\left(-\Omega_n t_n'\right)\right]$$

$$\times \eta\left(t_n'\right) \sum_{m=1}^{4} \frac{I_m}{|I_1|}\exp\left(-\omega_m t_n'\right), \tag{3.10}$$

where $t_n' = t - (n-1)\,t_0$ and $\eta(x)$ denotes the step-function, i.e., $\eta = 1$ if $x \geq 0$ and $\eta = 0$ if $x < 0$.

Taking the numerical values $l_1 = 4\,\mathrm{km}$, $\Delta l = 1\,\mathrm{km}$ and above-mentioned parameters of the return stroke, one can estimate the typical magnitude of the magnetic moment of the multiple return stroke as $M \sim 10\text{--}10^2\,\mathrm{kA\,km}$. Model calculation of the flash current moment for $n_0 = 3$ is shown in Fig. 3.9.

The spectrum of the current moment $MF(t)$ is given by

$$MF(\omega) = V_0 \sum_{n=1}^{n_0}\sum_{m=1}^{4} \frac{I_m \exp\left[i\omega t_0(n-1)\right]}{(\omega_m - i\omega)(\Omega_n + \omega_m - i\omega)}. \tag{3.11}$$

Figure 3.10 shows model calculation of the absolute value of the spectrum $MF(\omega)$ originated from $n_0 = 3$ return strokes, which follow one by one with equal interval $t_0 = 40\,\mathrm{ms}$. In such a case the spectrum has approximately a quasi-oscillatory profile with maximum repetition period about 25 Hz. This peculiarity of the spectrum is due to the presence of imaginary exponents in Eq. (3.11) and thus it follows from the interference between the fields of individual return strokes (e.g., see Surkov et al. 2010). Actually the number of strokes and intervals between their occurrence are rather random values that may result in randomizing of these oscillations.

Fig. 3.9 Model calculation of current moment of a multiple return stroke versus time
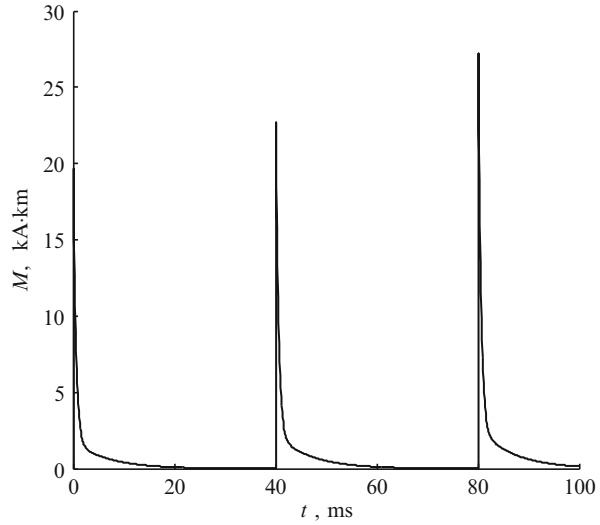

Fig. 3.10 Model calculation of the absolute value of current moment spectrum of multiple return strokes
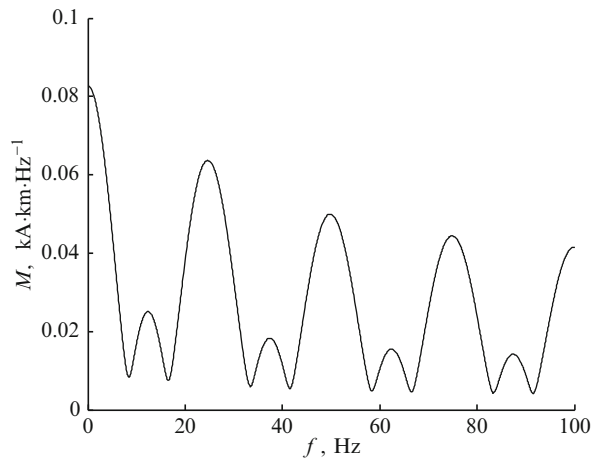
3.1.6 Global Thunderstorm Activity

Considering that there are perhaps 2,000 thunderstorms in progress around the world at any time, the measurements show that slow diurnal variations of the Earth electric field are in a good agreement with the variations of the global thunderstorm activity. Worldwide, both the Earth field and thunderstorm activity vary within $\pm 15\%$ and reach the peak value approximately at the same period from 14 UT till 20 UT. In particular, the diurnal variations of the Earth electric field correlate with diurnal variation of the global thunderstorm activity (e.g., see Bering et al. 1998; Füllekrug et al. 1999; Rycroft et al. 2000).

The weather condition and climate peculiarities may greatly affect the distribution of lightning discharges over the Earth surface. The thunderstorm cells more
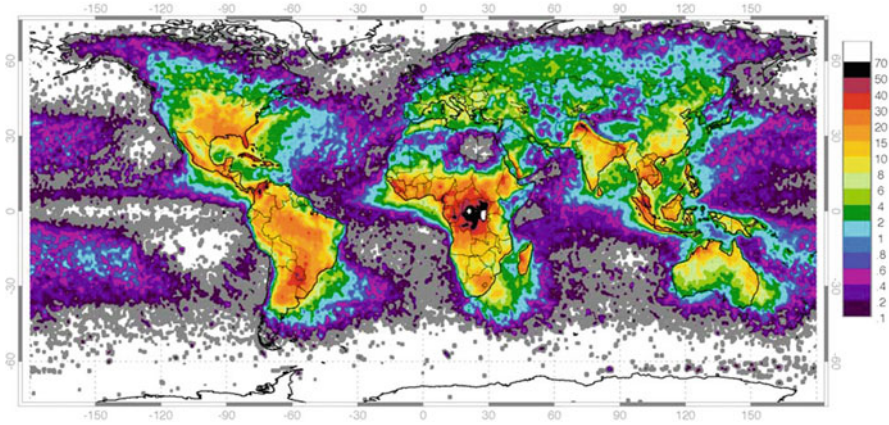
Fig. 3.11 NOAA satellite data of worldwide average annual lightning flashes per square kilometer. Taken from the site http://www.boqueteweather.com/lightning_year.htm

frequently occur in the regions covered with cyclones, typhoons, frontal zone of temperature inversion, climatological fronts and etc. (Watt 1967; Bhartendu 1969; Uman and Krider 1982; Uman 1987; Nickolaenko and Hayakawa 2002; Rakov and Uman 2003). The most favorable areas for the thunderstorm formation are usually associated with such regions as mountain ridges, which may affect the monsoon circulation, the river basins and bottom-lands, where the humid climate is predominant. Additionally, the group of islands in an ocean may influence the wind system in such a way that the wind system in this region is capable of sustaining the generation of thunderstorm clouds (Watt 1967). Based on observational data gathered for a long period one can characterize the lightning activity over the Earth surface through the mean number of flashes per unit of square in a year or month. An example of annual pattern of lightning activity over the globe as observed from space by the OTD is displayed in Fig. 3.11. The number of lightning per square kilometer in a year is shown with different colors. There is a small wonder that the main centers of lightning activity, termed global thunderstorm centers, are concentrated in tropics and around the equator. As is seen from Fig. 3.11, such centers cover three broad continental tropical regions, (1) the sub-Saharan Africa; (2) Central America and the Amazon basin in South America; and (3) the Malaysian Archipelago/Maritime continent extending from Southeast Asia across the Philippines, Indonesia, and Borneo into Northern Australia.

The number, ν, of lightning discharges per one km squared in a year inside these global thunderstorm centers is greater than 25 $km^{-2} \cdot year^{-1}$ (Bliokh et al. 1980). The value $\nu = 2.5$–7.5 $km^{-2} \cdot year^{-1}$ is typically for the regions with an enhanced lightning activity, while the regions with a moderate thunderstorm activity can be characterized by the value $\nu = 1.5$–2.5 $km^{-2} \cdot year^{-1}$.

The global thunderstorm centers play a crucial role in the formation of global electric circuit of the Earth. It is commonly accepted that the total electric current

arising from the global lightning activity must nearly cancel the inverse background atmospheric current, which is distributed around the whole globe. The global electric circuit is capable of sustaining both a constant potential difference between the Earth and the ionosphere and the fair weather electric field near the Earth surface.

3.2   Sprites, Blue Jets, and Other High Altitude Electric Discharges

3.2.1   Classification of TLEs

Gigantic electric discharges, also known as TLEs occur above a large thunderstorm at stratospheric and mesospheric altitudes. Since their recent discovery (Franz et al. 1990), much emphasis has been put into studies of these pleasing phenomena in the ground-based observations (e.g., Neubert et al. (2008) and references herein) as well as in the aircraft (Sentman and Wescott 1993; Sentman et al. 1995; Wescott et al. 1995), satellite (Chern et al. 2003; Mende et al. 2005; Cummer et al. 2006a; Chen et al. 2008), and space shuttle measurements (Boeck et al. 1992; Yair et al. 2004).

In a broad sense, the term TLEs includes not only the gigantic electric discharges but also a few extremely fast and highly dynamical electrical and optical phenomena which arise between the top of the thundercloud and the ionosphere. Depending on their properties the TLEs may be categorized by several types which are sprites/red sprites, blue jets (BJs), halos, elves and recently discovered blue starters and gigantic jets (GJs) (e.g., see Chen et al. 2008). The ISUAL satellite measurements have shown that the global occurrence rate of elves, sprites, halos, and GJs can be estimated as 3.23, 0.50, 0.39, and 0.01 events per minute, respectively. We cannot come close to exploring these topics in any detail since the main scope of our study is the low frequency effects associated with the TLEs. The reader is referred to the reviews by Ebert and Sentman (2008), Pasko (2010), Surkov and Hayakawa (2012) and Pasko et al. (2013) for the details on basic features of TLEs. However before discussing these effects, we need to understand a little about the underlying mechanisms of the TLEs.

The sprite is a luminous red glow occurring at 50–90 km altitude range with gradually changing to blue color below 50 km. As is seen from Fig. 3.12, the typical sprite consists of the upper diffuse region in red color and lower tendril-like filamentary structure in blue color with lateral dimension from 20–30 km to 50–100 km (e.g., Pasko 2006; Neubert et al. 2008; Stenbaek-Nielsen and McHarg 2008; Montanyà et al. 2010). Figure 3.13 shows that the visible inner structure of the tendrils and branches is very complicated. The bright streamer heads, shown with red color, vary in size from ~ 10 to ~ 100 m. This picture is highly dynamical since the streamer heads move in different directions at velocities about 10^3–10^4 km/s (Stenbaek-Nielsen et al. 2007). Typically, the sprite flash is lasted from a few to several tens of ms. The sprite halos have been occasionally observed approximately 1 ms prior to the sprite occurrence. The typical halo is visible as a ring area with 50 km diameter and 10 km thickness.
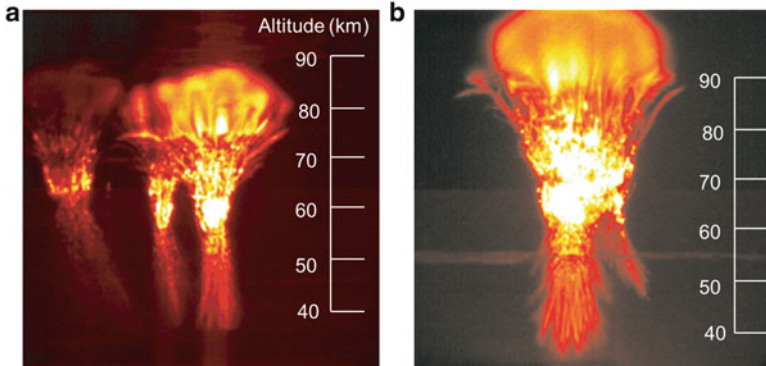
Fig. 3.12 The images illustrating the spatial sprite structure and transition between diffuse and streamer regions in the sprites as observed (**a**) 04:36:09.230 UT and (**b**) 05:24:22.804 UT on August 18, 1999. Taken from Stenbaek-Nielsen et al. (2000)
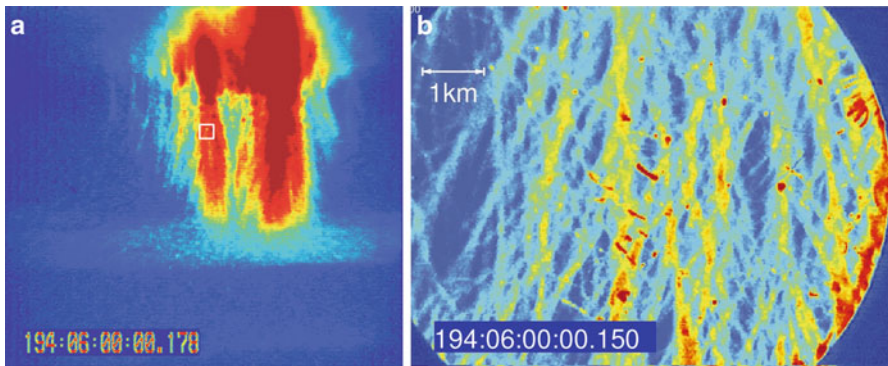
Fig. 3.13 Sprite telescopic images at low (**a**) and high (**b**) resolutions. The small area highlighted on the panel (**a**) is shown on the panel (**b**) at large scale. Taken from Gerken et al. (2000)

Blue jets (BJs) are beams of luminosity propagating upwards in narrow cones of about 15° from the tops of thunderclouds (e.g., Wescott et al. 1995; Boeck et al. 1995; Mishin and Milikh 2008). A color video imagery of the BJs has shown that this kind of TLEs exhibit primarily blue color. On average they are several km in diameter and typically brighter than sprites. BJs propagate with velocity of the order of 100 km/s, that is slower than sprites. They climb in the stratosphere up to 40–50 km altitude which implies a jet lifetime of 0.2–0.3 s. Blue starters are a kind of BJs which differ from them by a lower terminal altitude. They can develop upward from cloud tops at 17–18 km to terminal altitudes of about 25 km (Wescott et al. 1996; Heavner et al. 2000; Pasko 2006). Gigantic jets (GJs) are more intensive discharges with a much greater length than that of the BJs which results in the formation of electrical connection between thundercloud tops and the conducting E-layer of the ionosphere (Wescott et al. 2001; Su et al. 2003; van der Velde et al.
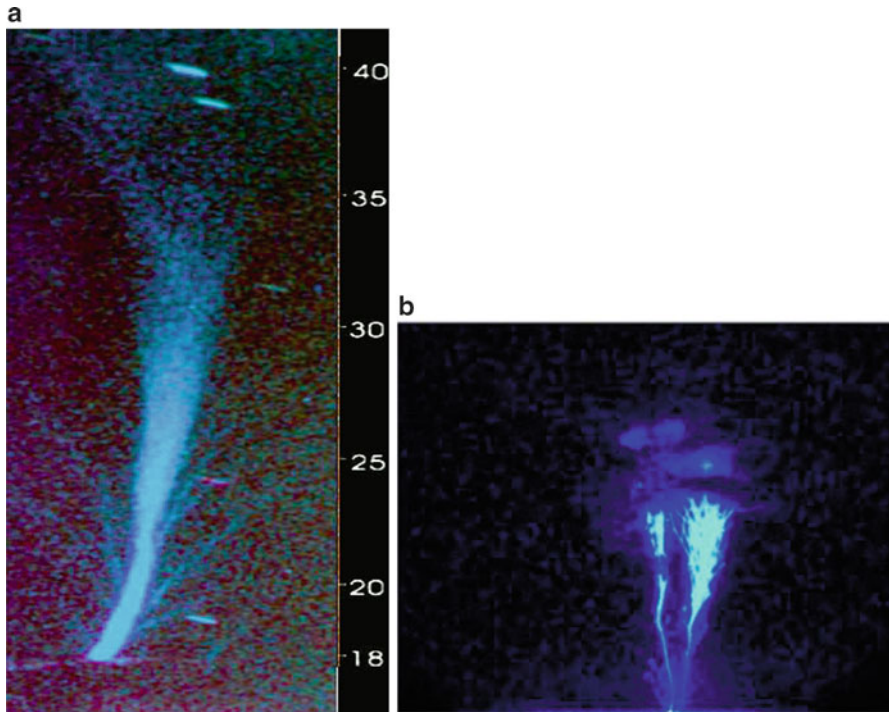
Fig. 3.14 Images of (**a**) blue jet (BJs) (Wescott et al. 2001), and (**b**) gigantic blue jet (GJ) (Pasko et al. 2002) discharged from the top of a thundercloud and upwards propagated to the lower ionosphere. The original images were recorded using a monochrome low-light video systems though the researchers observed the blue color flashes. To reproduce this effect, these images were enhanced with false color

2007; Kuo et al. 2009; Cummer et al. 2009). As illustrated in Fig. 3.14, the ground-based images of BJs and GJs exhibit a filamentary structure.

The predominance of red and blue colors in the optical emission of TLEs is believed to be due to the excitation of molecules of N_2 and O_2 by electron impact. At altitudes above 50 km the emissions of the first positive band of N_2 ($N_2 1P$) enhance a red optical region of red sprite emission whereas below 50 km the strong quenching of $B_3 \Pi_g$ state gives rise to the suppression of this emission. In the stratosphere the emission of the second positive band of N_2 ($N_2 2P$) becomes dominant, which results in predominance of blue color in the optical emission of BJs (e.g., see Vallance-Jones 1974; Pasko 2006, 2010). The recent high resolution measurements have shown that the most portion of the optical emission comes from the high-ionized streamer heads which manifest themselves as mobile bright compact balls (Liu and Pasko 2006; McHarg et al. 2007).

The elves are an abbreviation for Emission of Light and VLF perturbations due to EMP Sources (Fukunishi et al. 1996). The "elf" manifest itself as a divergent ring of optical emissions at the bottom of the ionosphere at ∼90 km altitude.

Typically the elves are visible for time interval less than 0.1 ms while their size can reach a value of 300–700 km in radius and 10–20 km in thickness. This short-term effect is associated with the ionospheric response to a strong electromagnetic pulse radiated by the CG discharge current of either polarity (e.g., see Boeck et al. 1992; Nickolaenko and Hayakawa 1995; Inan et al. 1996a, 1997; Cho and Rycroft 1998; Rowland 1998; Cheng et al. 2007).

Certainly, here we cannot come close to treating of other striking optical phenomena in the upper atmosphere such as trolls, gnomes, fairies, and so on.

3.2.2 Underlying Mechanisms for Blue Jets (BJs) and Gigantic Jets (GJs)

It is generally believed that BJs may occur under certain relatively rare conditions, when large amount of positive charge piles up at the top of thundercloud. Since the actual charge distribution in the cloud is very complicated we simplify the problem assuming as before that the charges are uniformly distributed in four spherical regions as shown in Fig. 3.3. According to this simplified model the dependence of the vertical field on altitude is described by the set of Eqs. (3.2)–(3.4). To simulate a quasielectrostatic (QE) field preceding a normal BJ discharge, Krehbiel et al. (2008) have suggested the set of parameters $q_i = 5, -40, 57.5$ and -20 C, where $i = 1, 2, 3, 4$. In Fig. 3.15, we plot the numerical calculation of the vertical field versus altitude based on the same parameters z_i and r_i as those used in making Fig. 3.4. It is obvious from this figure that the positive peak of E_z exceeds E_s^+ (line 2) around the altitude $z = 14$ km. On account of the positive field direction in this altitude range, we would expect the initiation of the upward-directed positive discharge which can propagate towards the ionosphere.

In this picture the BJ can be considered as upward-propagating positive leader with a streamer corona on the top (Petrov and Petrova 1999) as schematically displayed in Fig. 3.16. The streamer-to-leader transition is assumed to be accompanied by the Joule heating and subsequent electron detachment processes (Bondiou and Gallimberti 1994). So, more precisely, the BJs should be considered as hot leader-like discharges (Raizer et al. 2010) rather than cold streamer-like discharges, as the early modelers did. The leader bears a positive charge from the thundercloud top into the stratosphere up to altitude about several tens kilometers. A great number of the short-lived streamers are emitted from the leader thereby producing a streamer corona and a branching structure of BJ. However the leader velocity $\mathbf{V}_j$ is much less than that of individual streamers.

We have already discussed the scaling of critical breakdown field E_c which is proportional to the gas pressure and to the neutrals number density n_m at constant temperature. In a similar fashion the typical streamer parameters can be estimated on the basis of a similarity law and on dimension attributes (e.g., see Raizer et al. 1998; Pasko 2006; Surkov and Hayakawa 2012), according to which the typical
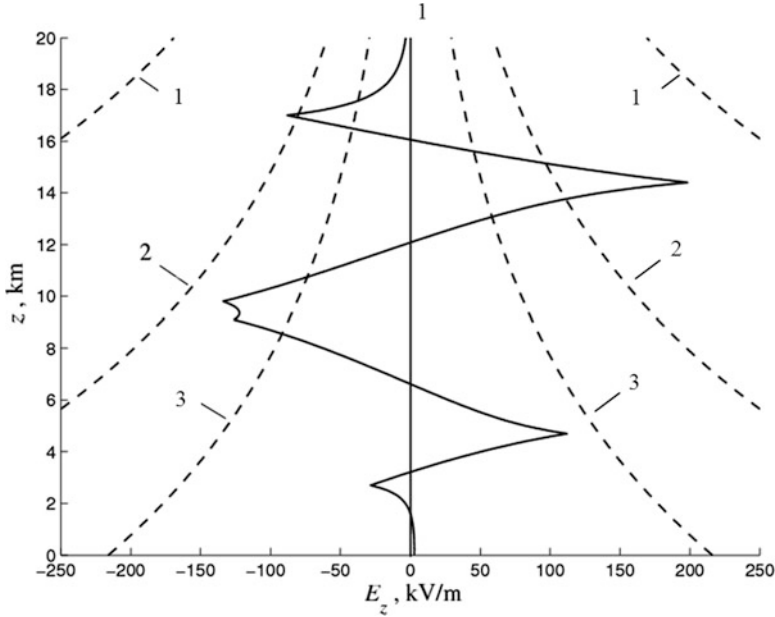
Fig. 3.15 The same as in Fig. 3.4 but for thunderstorm QE field preceding BJ discharge (Surkov and Hayakawa 2012)

discharge size L such as discharge tube length, streamer radius and etc. scales as $L \propto n_m^{-1} \propto \exp(z/H_a)$. Typical time interval T such as relaxation time, mean free time between collisions, two-body attachment time and etc. scales as $T \propto n_m^{-1}$. The typical velocity $V \propto L/T$ whence it follows that the streamer velocity, electron drift velocity V_d, and so on are independent of n_m whereas the electron mobility $\mu \sim V_d/E_c \propto n_m^{-1}$. Plasma and charge density inside the streamer body follows the scaling law: $n_e = n_i \propto n_m^2$ while the plasma conductivity scales as $\sigma \sim e n_e V_d \propto n_m$.

The increase in streamer size with altitude predicted by the scaling theory is compatible with the BJ observations. Although the similarity law for leader does not exist (Raizer 1991), with some care one may speculate that the conical shape of BJs and GJs (see Fig. 3.14) follows this similarity law since the scale of individual streamers and of the whole streamer zone has to increase with height. However, our calculations have demonstrated that the electric field produced by thundercloud charges is still smaller than that required for propagation of positive streamer (Fig. 3.15). Reasonable guesses as to the electrical inhomogeneity need to start breakdown ionization of the air. Another way of explaining this contradiction has been proposed by Raizer et al. (2006, 2007). In their model the BJ can be resulted from a bidirectional uncharged leader which in turn originates in the thundercloud area where the electric field reaches a maximum value. Owing to the exponential profile of the air density, the leader and the streamer corona are assumed to grow

Fig. 3.16 A scenario of BJ development considered as a positive leader-like discharge propagating upwards at the velocity $\mathbf{V}_j$ (Surkov and Hayakawa 2012)
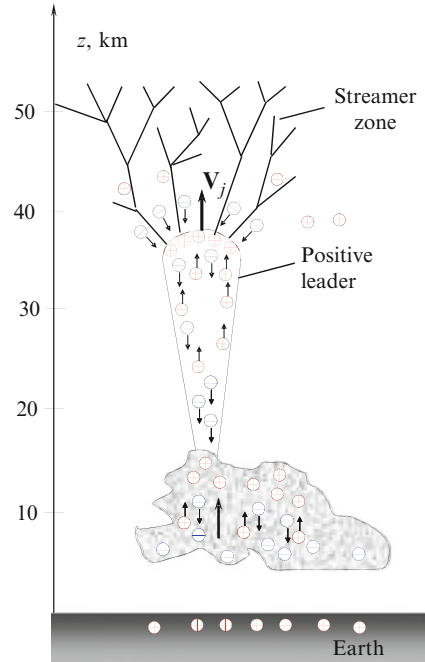
predominantly upward in contrast to laboratory conditions. Notice that the theory of streamers/leaders propagating at stratospheric and mesospheric altitudes is still far from being accurate.

It seems likely that the GJs can be associated with a large amount of negative electric charges accumulated at the middle region of thundercloud either by chance or as a result of another effect. One of the conceivable sets of the parameters for existence of this situation is as follows: $q_i = 25, -120, 82.5$ and -3 C (Krehbiel et al. 2008). A model calculation of the vertical QE field is presented in Fig. 3.17 as a function of height. The numerical values of other parameters used in making this plot are as follows: $z_i = 4.3, 8.0, 13.2, 15.4$ km, $r_i = 1.1, 2.6, 1.9, 0.3$ km. As is seen from this figure, the thunderstorm electric field is close to the breakdown threshold E_s^- (line 1) in the area above the charge $q_2 = -120$ C within the altitude range 10–12 km. This means that the GJ can be originated in this area as an upward-propagating IC discharge which transfers a negative charge of the order of 100 C through the region with upward/positive electric field towards the thundercloud top. Although the field is positive in a narrow region of 13–15 km above the charge $q_3 = 82.5$ C, the GJ can overcome this region to propagate out of the thundercloud towards the ionosphere (Krehbiel et al. 2008; Pasko 2010). However, we cannot explain in any detail why the GJs look more powerful than the BJs and why they can extend to higher altitudes.

It appears that the most of GJs develop in the form of upward-propagating negative leaders. In support of this conclusion it was noted that the visible
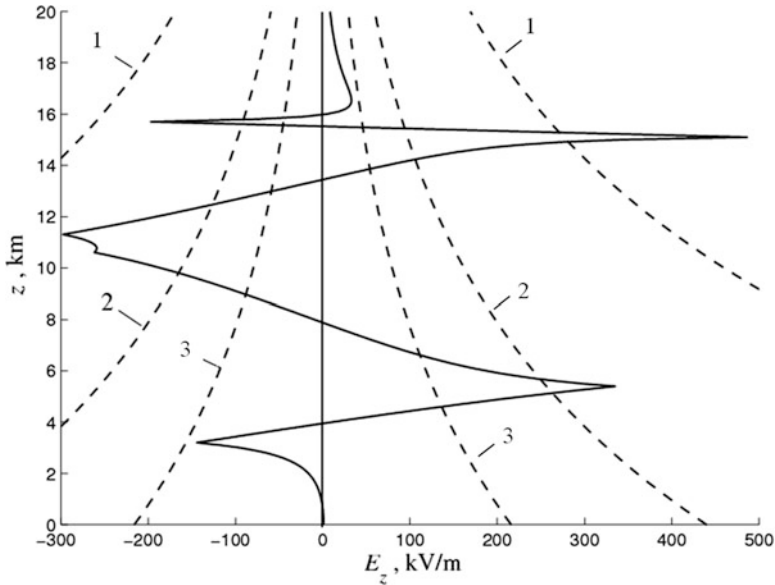
Fig. 3.17 The same as in Fig. 3.4 but for the thunderstorm QE field preceding a GJ discharge (Surkov and Hayakawa 2012)

patterns of GJs are similar to inverted images of conventional −CG (Pasko 2010; Neubert et al. 2011). Despite this similarity the other parameters of GJs differ significantly from those of standard −CG. For example, a GJ recently observed by Cummer et al. (2009) was estimated to transfer the negative charge of −144 C from the thundercloud to the lower ionosphere. This value is much greater than a typical charge ∼5–10 C lowered to the ground by a normal −CG stroke. Additionally, the onset time of the GJ current was about 30 ms which is much greater than that (∼5 μs) due to the stroke. This kind of GJ can be referred to as the class of negative cloud-to-ionosphere discharge (−CI)

The first documented event of positive cloud-to-ionosphere discharge (+CI) has been recently observed by van der Velde et al. (2010) during winter thunderstorms in the Mediterranean. This event is characterized by the current peak value of 3.3 kA and by short duration of 120–160 ms. This +CI discharge was estimated to lower negative charge −136 C down from the ionosphere to the positively charged origins in the cloud only 6.5 km tall that result in a huge charge moment change of 11,600 C km. This event has also demonstrated that high altitudes are not a necessary condition for initiation of GJs.

$t = 5.29$ ms $t = 5.71$ ms $t = 5.99$ ms $t = 6.41$ ms $t = 6.69$ ms $t = 6.96$ ms $t = 7.38$ ms $t = 10.29$ ms
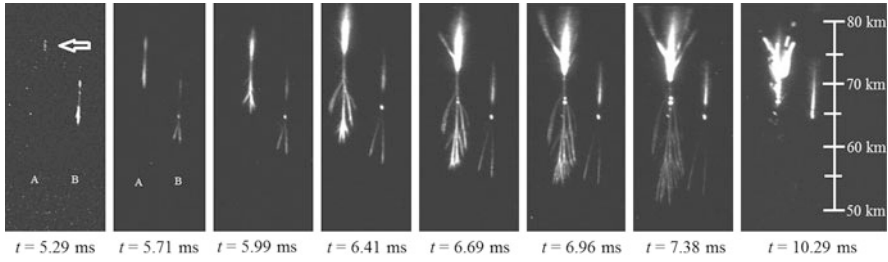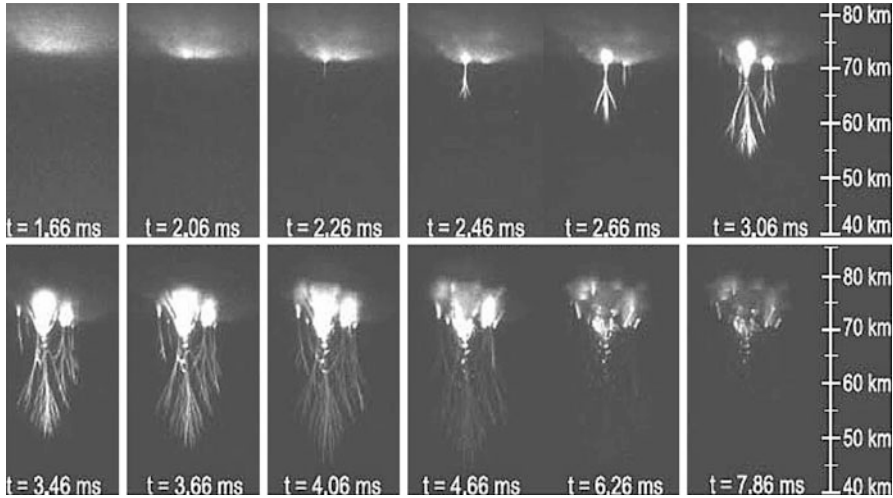
Fig. 3.18 High speed images of two sprites nucleation. The initiation point of the left sprite (*A*) is marked with an *arrow*. The images were recorded at Yucca Ridge Field Station on August 13, 2005 at 03:43:09.4 UT. The time was measured from the moment of lightning return stroke onset. The first image is contrast enhanced. Adapted from Cummer et al. (2006a)

3.2.3 Underlying Mechanisms for Sprites

A great deal of observations has shown that worldwide sprites and halos are triggered by large CG flashes almost exclusively with positive polarity (e.g., Boccippio et al. 1995; Williams et al. 2007). The charge moment change of the causative +CG was found to be greater than the critical value of the order of 500 C km in order to initiate the sprite discharge (Stanley et al. 2000; Cummer 2003; Cummer and Lyons 2005; Rycroft 2006; Hiraki and Fukunishi 2007). The high-speed video recording of sprites initiation has shown (Cummer et al. 2006b) that at first the downward streamer originates either spontaneously from a bright nucleolus between 70 and 75 km altitude (Fig. 3.18) or from brightening inhomogeneities at the bottom of a halo (Fig. 3.19). As is seen from the images shown in Fig. 3.18, the brighter column continues to expand upward and downward from the nucleation point followed by the generation of bright upward propagating streamers that branch and terminate in diffuse emissions. In the case shown in Fig. 3.19, at first the distinct bright nucleolus develop at the lower edge of the originally homogeneous halo. A downward streamer then initiates from that point thereby producing the bright column which in turn begins to expand upward and downward. The upward streamers propagate at velocity $(0.5–2) \times 10^4$ km/s and terminate in diffuse emissions as in the previous example (Stanley et al. 1999; Cummer et al. 2006b; Stenbaek-Nielsen and McHarg 2008).

It is generally accepted that there are two basic visible shapes of sprites: "carrot" or "jellyfish" configuration and columniform (e.g., Cho and Rycroft 1998; Matsudo et al. 2007; Myokei et al. 2009). The carrot type sprites are characterized by diffuse tops and lower tendrils extending down to altitudes of 30–40 km, while the columniform sprite has a very fine spatial structure as compared with the "carrot" sprite (e.g., Wescott et al. 1998; Hayakawa et al. 2004). It appears that these kinds of sprites differ in time delay with respect to a causative +CG. Winter thunderstorm observations in the Hokuriku area of Japan have shown that the "column" sprites

Fig. 3.19 High speed images of the sprite nucleation. The images were recorded at Yucca Ridge Field Station on August 13, 2005 at 03:12:32.0 UT. Adapted from Cummer et al. (2006a)

might be delayed by several ms after the causative +CG discharge while "carrot" sprites occur tens of ms after the +CG lightning (e.g., Matsudo et al. 2009; Suzuki et al. 2011).

The positive CG flashes may result in the extraordinary large charge transfer ($\sim$100 C) for the short time that gives rise to the strong QE field caused by uncompensated negative charges located in the thundercloud. To estimate this QE field at high altitudes, consider first a short period just after the causative +CG lightning. In the first approximation this implies that the conduction current, $\sigma_a E$, is much smaller than the displacement current, $\varepsilon_0 \partial_t E$, so that the air conductivity can be neglected. To simplify the problem, the thundercloud charge is assumed to be uniformly distributed inside the ball with radius r. The center of the charged ball is located on z-axis at the altitude h above the perfectly conducting ground. In this model the vertical component of electric fields E_z on z axis is described by equations similar to Eqs. (3.2)–(3.4). The thundercloud charge q and QE field can gradually increase just after the moment of main stroke due to strong CC in the sprite-associated +CG lightning. This CC is normally much greater than that due to negative stroke and its value amounts to 5–10 kA for a relatively long period of 10–100 ms (Rakov 2000). To illustrate this tendency, plots of E_z versus altitude z are shown in Fig. 3.20 with lines 1–3, which correspond to $q = 50$, 100, and 150 C, respectively. In making these plots the numerical values $h = 10$ km and $r = 2$ km are used.

We recall that all the threshold fields exponentially decrease with altitude whereas the QE field caused by the thundercloud charge and its electric image in the conducting ground falls off according to the dipole law; that is, inversely as the cube of the distance from the source. This means that the breakdown fields decrease
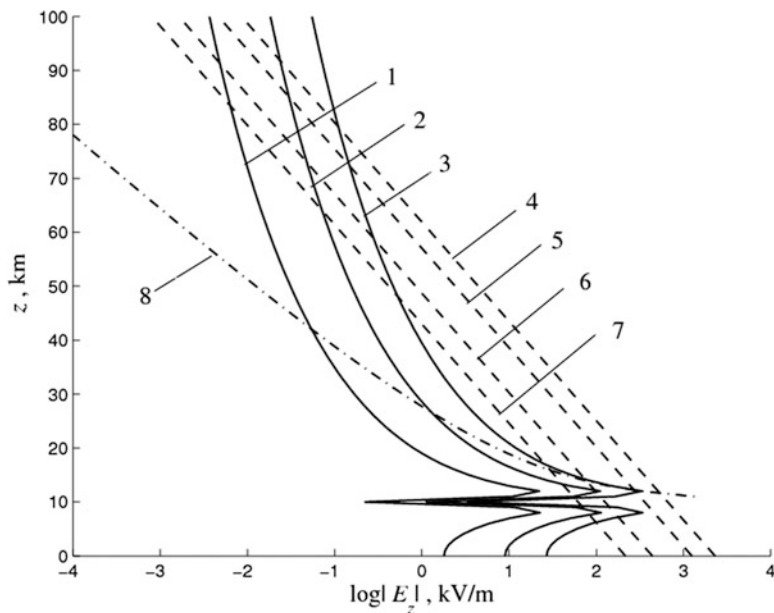
Fig. 3.20 Model calculations of thundercloud QE field just after a strong +CG which is able to trigger sprite discharge. The absolute value of the vertical electric field for different thundercloud charge q is plotted in this figure with lines 1–3 and 8 as a function of altitude: 1—$q = 50$ C; 2—$q = 100$ C; 3 and 8—$q = 150$ C, respectively. In making the plots 1–3 the air conductivity was ignored. The breakdown threshold electric fields which correspond to different air breakdown criteria are shown with dotted lines: 4—conventional breakdown threshold, 5—negative streamer propagation, 6—positive streamer propagation, 7—relativistic runaway breakdown. *Dash-and-dot line 8* illustrates the air conductivity effect on thunderstorm QE field (Surkov and Hayakawa 2012)

with altitude more rapidly than does the thunderstorm electric field. So, there may be a height above which the thundercloud electric field exceeds the breakdown threshold (Wilson 1925). As is seen from Fig. 3.20, this situation may exist at the mesospheric altitude range 50–80 km.

Actually, the generation of QE electric fields above a thundercloud may be greatly reduced due to the exponential increase of the atmospheric conductivity with altitude. The background atmospheric conductivity is a subject of a variety of factors: cosmic-ray ionization rate, ion–neutral collision rate, electron attachment and detachment and etc., which in turn vary with altitude due to changes of the air density. However in the first approximation the air conductivity can be approximated by Eq. (3.1); that is, as an exponential function of altitude z. The thundercloud charge variations, which follow primary +CG stroke, are basically due to the CC. However, if the time scale of the charge variations is much greater than the relaxation time $\tau = \varepsilon_0/\sigma_a$ due to air conductivity, then the problem is reduced to a stationary one. In this extreme case a distribution of electric potential

Φ is described by Poisson equation. Considering the thundercloud as a point current source located on z-axis at the altitude h, we come to the following equation:

$$\frac{\sigma_a}{r} \partial_r \left(r \partial_r \Phi \right) + \partial_z \left(\sigma_a \partial_z \Phi \right) = \frac{I \delta \left(r_- \right)}{4 \pi r_-^2}, \tag{3.12}$$

where I denotes the total current flowing from the source, δ stands for Dirac delta-function, and $r_\mp = \left\{ r^2 + (z \mp h)^2 \right\}^{1/2}$. This equation should be supplemented by the proper boundary conditions for the conducting ground and at the infinity, that is, $\Phi = 0$ at $z = 0$ and $\Phi \rightarrow 0$ when $z \rightarrow \infty$. Substituting the relationship $\sigma_a = \sigma_0 \exp \left(\alpha z \right)$ into Eq. (3.12) and solving the problem gives (e.g., see Soloviev and Surkov 2000)

$$\Phi = \frac{I}{4\pi\sigma_0} \exp \left[-\frac{\alpha}{2} \left(z + h \right) \right] \left\{ r_-^{-1} \exp \left(-\frac{\alpha r_-}{2} \right) - r_+^{-1} \exp \left(-\frac{\alpha r_+}{2} \right) \right\}. \tag{3.13}$$

The total charge q of the source/thundercloud can be related to the source current I through the Gauss theorem and Ohm law whence it follows that $I = (q\sigma_0/\varepsilon_0) \exp \left(\alpha h \right)$. When $\alpha = 0$, Eq. (3.13) describes a potential of point charge q and its mirror image in the perfectly conducting ground. In general case the exponential factors in Eq. (3.13) lead to the strong field attenuation with altitude due to air conductivity.

   This model with the parameter $\alpha = 0.15 \, \text{km}^{-1}$ and $q = 150 \, \text{C}$ was used for numerical calculation of the vertical component of the thundercloud electric field $E_z = -\partial_z \Phi$ along z-axis in the presence of atmospheric conductivity as shown in Fig. 3.20 with dash-and-dot line 8. The role of the atmospheric conductivity comes into particular prominence when comparing this graph with that calculated at the same thundercloud charge and zero atmospheric conductivity (line 3). It is obvious from Fig. 3.20 that the conduction current due to the atmospheric conductivity may decrease the thunderstorm field to such an extent that it makes impossible the air breakdown in the mesosphere. In a more accurate model which takes into account both the time-dependent CC and the air conductivity, the altitude profile of the electric field be situated between lines 3 and 8 (Mareev and Trakhtengerts 2007). In this notation, the sprites must build up very quickly just after the causative lightning discharge for the short period limited by the relaxation time τ that varies within 1–100 ms in the altitude range 60–80 km.

   The sprite initiation, visible evolution, streamer structure, and their relationship with IC process are so complex that any quantitative theory of the sprites has not been established yet except a number of numerical simulations (e.g., Pasko et al. 2000, 2001; van der Velde et al. 2006, 2007; Asano et al. 2009a,b; Ebert et al. 2010).

   Luque and Ebert (2009, 2010, 2012) have recently developed a numerical model of sprite initiation that takes into account the photoionization effect and altitude-dependent transport and ionization parameters of electrons and neutrals. This model does not require any kind of seed electrons since the primary streamer is assumed to be due to drift of the background electrons subjected to thundercloud electric field.

Fig. 3.21 A schematic plot
of sprite originated from a
sprite halo in the presence of
QE field generated above a
thundercloud after +CG
lightning (Surkov and
Hayakawa 2012)
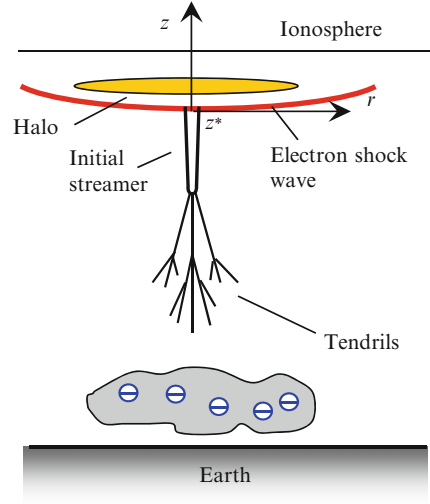
Their numerical simulations show that (1) several ms after the powerful causative
+CG lightning a downward-propagating electron density shock wave can develop
in the lower ionosphere, (2) then this wave transforms into the downward self-
propagating narrow filament which can serve as a positive sprite streamer, and (3)
the impact and photo-ionization rates are the highest at the streamer head. In this
model the electron density wave can be considered as a possible candidate for the
visible sprite halo.

To give a qualitative interpretation of these results, we assume that a dipole
approximation could be applied to mesospheric electric field of the thundercloud
charges and of their mirror image in the perfectly conducting ground

$$E = \frac{d}{4\pi\varepsilon_0 (r^2 + z^2)^{3/2}} \left(1 + \frac{3z^2}{r^2 + z^2}\right)^{1/2}, \tag{3.14}$$

where r and z are cylindrical coordinates which are shown in Fig. 3.21. The electric
dipole moment $d = 2qL$, where q is the thunderstorm charge and L is the
distance from the thundercloud to the ground. We also assume that the thundercloud
electric field at the front of the electron wave is close to the breakdown threshold.
Substituting Eq. (3.5) for E into Eq. (3.14) gives the implicit dependence $r(z)$ or
$z(r)$, which defines the surface of the wave front. This surface crosses z axis at the
point z_* which can be found from the following equation

$$\frac{d}{2\pi\varepsilon_0 z_*^3} = E_0 \exp\left(-\frac{z_*}{H_a}\right). \tag{3.15}$$

In the vicinity of the axis of symmetry ($r \ll z$) the relationship between r and z can be simplified in such a way that we come to the explicit dependence $r(z)$ which is valid as $z \geq z_*$:

$$r = 4z \left\{ \frac{\pi \varepsilon_0 E_0}{15d} \left[z_*^3 \exp\left(-\frac{z_*}{H_a}\right) - z^3 \exp\left(-\frac{z}{H_a}\right) \right] \right\}^{1/2}. \qquad (3.16)$$

The wave front given by Eq. (3.16) is schematically shown in Fig. 3.21 with red line. It follows from Eq. (3.15) that an increase in dipole moment d results in a decrease of z_*. This means that the enhancement of thundercloud field is accompanied by downward propagation of the point z_* and the wave front given by Eq. (3.16). Although this qualitative analysis is consistent with the results of numerical simulations reported by Luque and Ebert (2009), the above approach cannot predict the sharp prominence arising in the center of the wave surface because we have ignored the electric field of charges accumulated at the wave front. This point requires the precise analytical analysis because this effect can be due to plasma or other kind of instabilities (e.g., Derks et al. 2008).

3.2.4 Runaway Electron Breakdown

As has already been discussed, the conventional streamer-leader mechanism for air breakdown can explain, in principle, the basic properties of the TLEs (e.g., see Riousset et al. 2010a,b; Raizer et al. 2010). An alternative approach assumes the relativistic runaway electron avalanches as the proper candidate for producing the air breakdown at stratospheric and mesospheric altitudes (e.g., see Gurevich et al. 1992, 1994; Roussel-Dupré and Gurevich 1996; Lehtinen et al. 1997, 1999; Babich et al. 1998, 2008; Gurevich and Zybin 2001; Lehtinen 2000; Füllekrug et al. 2010, 2011). One of the merits of this mechanism is that the electric field threshold required for air breakdown may be one order of magnitude lower than that due to the conventional breakdown.

In the course of this text, the runaway breakdown is only treated in a sketchy fashion. First of all we note that if the electron energy greater than 50 eV then there prevails the electron forward scattering at small angles. In this notation we consider the simple one-dimensional model in which all the high-energy electrons can move only along z axis parallel to the constant electric field $\mathbf{E}$. The electron collisions are taken into account by means of the so-called dynamical friction force F_{fr} which is pointed oppositely to the vector of electron momentum $\mathbf{p}$. In such a case the equation of electron motion is reduced to the following (Gurevich et al. 1992, 1994)

$$\frac{dp}{dt} = eE - F_{fr}. \qquad (3.17)$$

In a more accurate model one should take into account the angle included between the electric force eE and the electron momentum.

The dynamical friction force is equal to the electron energy loss due to the electron collisions per unit length, that is,

$$F_{fr}(\varepsilon) = \frac{d\varepsilon}{dz}. \tag{3.18}$$

A main contribution to the energy losses from high-energy electrons is caused by the ionization of air. A peculiarity of this ionization process is that the energy of the fast-moving electron is much greater than the energies of atomic electrons. This means that the high-energy electron interacts with atomic electrons and nuclei as with free particles. In such a case the friction force can be estimated as $F_{fr}(\varepsilon) \sim \varepsilon/\lambda$, where the free length of the electrons $\lambda \sim (Z n_m \sigma_c)^{-1}$ depends on the number density of molecules n_m, the mean number of electrons in molecule Z, and the scattering cross section σ_c. In the non-relativistic energy range the interaction between charged particles is governed by the Coulomb law through Rutherford scattering cross-section $\sigma_c \sim e^4/\varepsilon^2$ (e.g., see Gurevich and Zybin 2001). Combining the above relationships, we arrive at the following estimate $F_{fr}(\varepsilon) \sim e^2 Z n_m/\varepsilon$. Notice that this dependence is in good agreement with the equation derived by Bethe (1930) in a more accurate model:

$$F_{fr}(\varepsilon) = \frac{2\pi e^4 Z n_m}{\varepsilon} \ln \frac{\varepsilon}{J_z}. \tag{3.19}$$

Here $J_z \sim \varepsilon_i$, where ε_i is the energy of ionization.

A schematic plot of the dynamical friction force of electrons as a function of their kinetic energy is displayed in Fig. 3.22. Here we do not show a few resonance peaks in the low-energy region although on average the friction force approximately increases in this region as shown with dashed line. As is seen from this figure, the friction force reaches a maximum value at the energy ε_*. This maximum corresponds to the so-called thermal runaway breakdown threshold, which occurs at the electric field $E_{th} \approx 260\,\text{kV/cm}$. So large electric field does not occur at stratospheric and mesospheric altitudes.

Equation (3.19) can be applied to the 10^2–10^6 eV energy range where the friction force falls off with increasing the electron energy. At higher energies one should take into account relativistic effects which were ignored in deriving the above estimates. The contribution of the relativistic effects results in gradual changes in the above tendency in such a way that the friction force reaches a minimum $F_{\min}$ at the energy $\varepsilon_{\min} \approx 1.4\,\text{MeV}$, and then a logarithmically slow increase begins to prevail at higher energies (Gurevich and Zybin 2001).
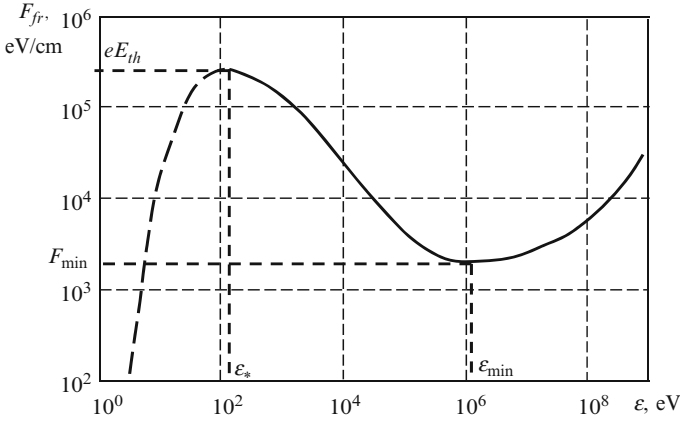
Fig. 3.22 A schematic plot of dynamical friction force of electrons in the air versus electron kinetic energy. The figure is partly adapted from Pasko (2006)

The generation of the runaway electrons is possible in the energy range from ε_* to $\varepsilon_{\min}$ where the fall off of the friction force dominates. It follows from Eq. (3.17) that the runaway electrons can appear under the requirement

$$eE > F_{fr}(\varepsilon). \tag{3.20}$$

which means that the electric field will accelerate the electrons with such energies continuously so that they become "runaway" electrons. The implication here is that the increase of the electron energy in the electric field prevails over the energy losses due to ionization of air. Conversely, if $eE < F_{fr}(\varepsilon)$, then the electron energy falls off quickly due to the ionization of air and other inelastic processes result in the energy losses. The requirement given by Eq. (3.20) can be satisfied for the ambient electric field $E > E_r = F_{\min}/e$. It follows from the detailed analysis that the minimal value of the threshold electric field is given by (Gurevich and Zybin 2001)

$$E_r = \frac{4\pi e^3 Z n_m a}{m_e c^2}, \tag{3.21}$$

where the dimensionless parameter $a \approx 11$.

To satisfy Eq. (3.20), the runaway electron energy must be greater than the threshold value, ε_r, which depends on the ambient electric field. Combining Eqs. (3.19)–(3.21) we obtain that

$$\varepsilon > \varepsilon_r \approx \frac{m_e c^2 E_r}{2E}. \tag{3.22}$$

Runaway electron propagation through the air is accompanied by the generation of large amount of secondary low-energy electrons due to the neutral molecule ionization by runaway electron impact. Although a majority of secondary electrons have a small energy, a portion of such electrons may gain energy ε which is greater than the threshold value; that is, $\varepsilon > \varepsilon_r$. The ambient electric field will accelerate these energetic electrons, so that they may also become runaway electrons, which in turn results in additional ionization of air and the generation of a new portion of secondary and runaway electrons. The exponentially increasing avalanche of runaway electrons is a crucial factor in the development of air breakdown since a great deal of the secondary slow electrons is produced along with the runaway electrons (e.g., see Colman et al. 2010).

It follows from Eq. (3.21) that the runaway breakdown field E_r is proportional to the neutral number density. Taking the notice of Eq. (2.3) for n_m gives the following approximation (Gurevich and Zybin 2001):

$$E_r = 2.16 \exp\left(-z/H_a\right), \quad \text{kV/cm.} \tag{3.23}$$

It should be emphasized that the value of the runaway breakdown threshold E_r is one order of magnitude smaller than the conventional breakdown E_c. This important fact follows from a comparison of Eqs. (2.3) and (3.23). The runaway breakdown field E_r is shown in Figs. 3.4, 3.15 and 3.17 with line 3. On the other hand, the thermal runaway breakdown threshold $E_{\text{th}} \approx 260\,\text{kV/cm}$ is approximately 100 times greater than the runaway threshold E_r. Under such a strong electric field all the thermal electrons become runaway ones since the electric force acting on electrons becomes greater than the maximal dynamical friction force shown in Fig. 3.22. A more sophisticated treatment has shown that as the electric field E is close to the breakdown threshold then the characteristic length l_r of runaway electron avalanches is inversely proportional to n_m (Gurevich and Zybin 2001). Since the neutral number density decreases with altitude, the value of l_r, on the contrary, increases from several tens meters at the ground surface level to a few km at the mesospheric altitudes. It is obvious from Fig. 3.20 that the thundercloud electric field arising after a CG discharge (lines 1–3) can exceed the runaway breakdown threshold (line 7) in the tens km altitude range which is greater than the length l_r of exponential growth of runaway electron avalanche.

Radiations of relativistic electrons give rise to the generation of Roentgen and gamma quanta which in turn are able both to ionize the molecules and to generate electron–positron pairs when interacting with nuclei of molecules. In the course of this text, we cannot come close to exploring these topics owing to the complexity of this problem. In a more accurate theory, the Boltzmann transport equation is used to describe the runaway electron distribution function $f\,(\mathbf{r}, \mathbf{p}, t)$ in phase space (e.g., see recent reviews by Roussel-Dupré et al. (2008) and by Milikh and Roussel-Dupré (2010))

$$\partial_t f + \mathbf{V} \cdot \nabla f + e\mathbf{E} \cdot \nabla_{\mathbf{p}} f = S\,(f, f_n), \tag{3.24}$$

where $\nabla_{\mathbf{p}}$ denotes gradient with respect to components of the momentum $\mathbf{p}$. Here the collision integral S is dependent on the distribution functions of electrons f and neutral molecules f_n. The interested reader is referred to a discussion by Gurevich and Zybin (2001) and by Trakhtengerts et al. (2002, 2003) for details about solutions of this equation.

The models of runaway breakdown in the atmosphere are based on the assumption that cosmic rays generate a shower of secondary particles, called an extensive air shower (EAS), thereby producing seed/secondary relativistic electrons which are capable of initiating the runaway breakdown in the presence of a strong QE field of thundercloud (Gurevich et al. 1999; Lehtinen et al. 1999; Gurevich and Zybin 2001, 2004; Inan and Lehtinen 2005; Roussel-Dupré et al. 2008; Milikh and Roussel-Dupré 2010). The incident cosmic ray particle energy to initiate runaway breakdown was estimated to be greater than or of the order of 10^{15} eV (Gurevich et al. 1999). The EAS typically consists of 89 % photons, 10 % electrons with the energy up to 30 MeV and 1 % other particles, largely muons (e.g., Carlson et al. 2008).

Modeling of interference between electromagnetic wave radiated by the horizontal branch of the parent lightning discharge and the waves reflected from the night ionosphere and the ground has shown that the transient electric field in the mesosphere can exceed the runaway electron threshold that supports the idea of free electron bunching in the mesosphere by the pulsed electric field (Kudintseva et al. 2010).

The numerical simulation has shown that one more conceivable reason for the existence of runaway is the electron acceleration during the propagation of lightning streamers and stepped leaders (e.g., Gurevich et al. 2007; Carlson et al. 2010; Chanrion and Neubert 2010; Celestin and Pasko 2011). The secondary fast electrons with the MeV energies may come out from the radioactive decays of a rest muon after an IC lightning discharge (Paiva et al. 2009).

Despite the threshold E_c for conventional breakdown is approximately an order of magnitude greater than that for runway breakdown, the focusing of the electric field in the vicinity of any inhomogeneity could lower the value of E_c by a factor of 10 or 30 (Fernsler and Rowland 1996) and vice versa, the actual field needs to be two to three times the runaway threshold E_r to get sufficient ionization for starting of runaways (Rowland 1998). It may be suggested that the conventional and runaway breakdowns develop at different altitudes, which are separated by only a few kilometers. Once either process is triggered prior to the next one, it can suppress the other process from triggering because of fast electric field relaxation due to the air polarization caused by the increase of plasma density. This implies that there may be a hybrid sprite model in which both the breakdown mechanisms may occur simultaneously (Roussel-Dupré and Gurevich 1996; Yukhimuk et al. 1999; Li et al. 2009, 2010; Chanrion and Neubert 2010).

An observational hint toward the runaway electron mechanism does occur in the atmosphere is the observations of the so-called terrestrial gamma ray flashes (TGFs); that is, short bursts of gamma rays originating from Earth's atmosphere. These events are believed to be due to Bremsstrahlung emissions from energetic (∼1 MeV) electrons interacting with neutral molecules (e.g., see; Dwyer et al. 2010;

Carlson et al. 2010). Since their experimental finding (Fishman et al. 1994), the TGFs have been studied intensively for the last decades and much is now known of their properties. Typically, the TGFs occur in the form of narrow beams with energies up to 20 MeV and duration from 0.2 to 3.5 ms. It is generally believed that the TGFs are associated with an individual lightning strike though the observed rate of TGF events is much smaller than that of lightning flashes (Fishman et al. 1994; Inan et al. 1996b; Inan and Lehtinen 2005; Cummer and Lyons 2005; Smith et al. 2005, 2010; Briggs et al. 2010). This fact can be due to difficulties in detecting the TGFs.

3.2.5 VLF Probing of the Lower Ionosphere Above Thunderstorm: Early/Fast and Early/Slow Events

A major part of our knowledge of sprite properties is based on optical and spectral measurements, video observations of sprite morphology, and much was done for improvement of the spatial and temporal resolution of the sprites structure. Other instrumentations and technique are necessary to study the IC processes associated with the sprite evolution. The distribution of sprite delay between a sprite and its causative +CGs is indicative of correlation between IC processes and sprite generation mechanisms. Simultaneous optical and ELF/VLF observations are believed to be an effective technique for discussing the relationship between the sprite and its causative lightning (Füllekrug and Constable 2000; Sato and Fukunishi 2003; Hobara et al. 2006; Cummer et al. 2006a,b; Neubert et al. 2008; Surkov et al. 2010).

The ground-based narrowband VLF transmitters and receivers are commonly used to detect the perturbations of ionospheric and mesospheric conductivity caused by lightning discharges. This effect can be observed by distant measuring of the changes in the amplitude and phase of VLF electromagnetic wave propagating in Earth-Ionosphere waveguide and passing over a thunderstorm region (e.g., Dowden et al. 1996; Neubert et al. 2008). Design of the experiment scheme is shown in Fig. 3.23. The so-called lightning-induced electron precipitation effects (LEPs) or Trimpi effect are considered as a possible cause for this phenomenon (Helliwell et al. 1973). A portion of electromagnetic energy radiated by lightning penetrates through the ionosphere thereby exciting a whistler mode wave in the magnetosphere. As the Doppler-shifted frequency of the whistler mode wave is close to the gyrofrequency of trapped radiation-belt electrons then a resonance wave-particle interaction occurs which results in changing the electron pitch angle sufficiently to reduce it below the loss cone (Trakhtengerts and Rycroft 2008). As a result, the precipitation of 0.1–0.3 MeV electrons occurs at the base of the field line causing the local increase in the ionization and conductivity in D region of the ionosphere. The typical lateral size of the ionization region is about 1,000 km. The lag time between LEPs and the lightning is ∼1 s, and the onset time is about several seconds, while the recovery time varies within 10–100 s.
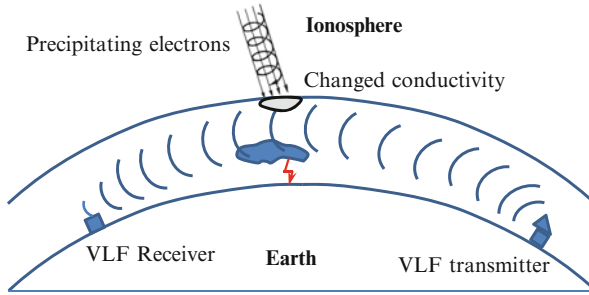
Fig. 3.23 Experimental scheme for remote measurement of the amplitude and phase changes of VLF electromagnetic wave propagating in the Earth-Ionosphere waveguide over a thunderstorm region. The local conductivity enhancement in the D region can be due to lightning-induced electron precipitation effects. The similar phenomena can be produced by the sprite ionization column and sprite halos in the D region

A similar effect associated with sprite-producing lightning is referred to as early/fast Trimpis (Inan et al. 1995). An example of the "early/fast" events observed in Crete during the 2003 EuroSprite campaign is displayed in Fig. 3.24. The observations have shown that sprites are nearly always accompanied by "early" VLF perturbations (Neubert et al. 2005, 2008). The lag time between the perturbations in signals from distant VLF transmitter and causative +CG lightning is less than 20 ms, that is shorter than the lag time observed during LEPs. Typically the onset time of the "early" perturbations is less than 50 ms while the recovery time varies within 10–300 s (Inan et al. 1995, 1996a, 2010; Hobara et al. 2001; Otsuyama et al. 2004; Neubert et al. 2008). Most of "early" VLF events are supposed to be due to the region of enhanced conductivity produced by the sprite ionization column and sprite halos in the upper D region. The typical lateral size of this region is about 100 km.

To treat early VLF events associated with sprite discharges in the D region, we need a combined set of Maxwell and continuity equations for charged particles. These equations govern the dynamics at least four kinds of particles; that is, electrons, positive ions, negative ions, and positive cluster ions (e.g., Glukhov et al. 1992; Haldoupis et al. 2009). As is seen from Fig. 3.24, the early VLF perturbation is characterized by an abrupt signal onset and a long recovery. In what follows we focus on a more slowly recovery process. Thus far, no consideration has been given to the short-term stage of electron production and ionization in the lower ionosphere caused by impact of a causative lightning and its sprite. Considering the plasma recombination, the continuity equation for electrons can be thus written as

$$\frac{dn_e}{dt} = -\alpha_d n_e n_i - \alpha_d^c n_e n_x, \tag{3.25}$$

where n_e, n_i, and n_x stand for electrons, positive ions, and positive cluster ions number densities, respectively. Here α_d denotes the coefficient of dissociative
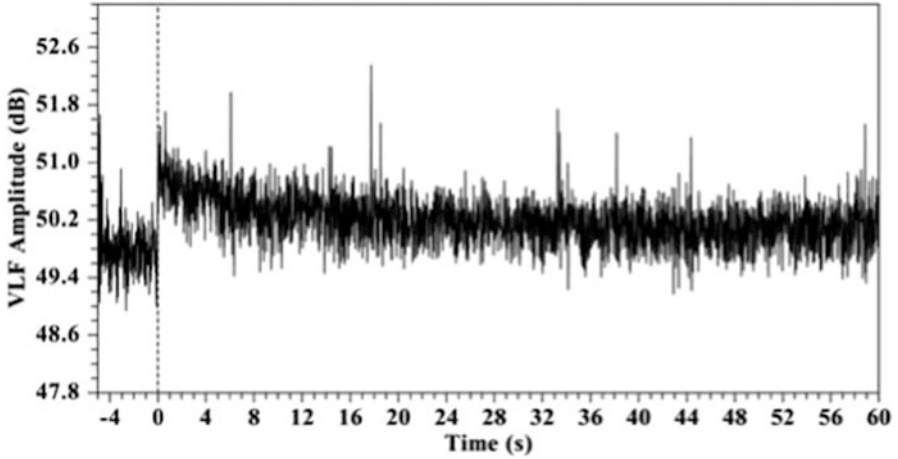
Fig. 3.24 A signature of "early/fast" VLF event associated with a sprite which was observed in Crete on August, 29 during the 2003 EuroSprite campaign (Neubert et al. 2005). Typically these events are characterized by an abrupt onset and a signal recovery ranging from 10–300 s. Adapted from Haldoupis et al. (2009)

recombination with positive ions, the majority of which compose O^{2+} and NO^+ while α_d^c is the effective coefficient of recombination of electrons with positive cluster ions which are produced from positive ions via a hydration chain reaction. Notice that the interaction between electrons and negative ions due to electron attachment and detachment does not enter this simplified equation.

Taking into account that the dissociative recombination of electrons and single positive ions dominates above 80–85 km (Glukhov et al. 1992; Haldoupis et al. 2009); that is, in the altitude range of interest, one may ignore the last term on the right-hand side of Eq. (3.25). Additionally, taking the notice of plasma quasi-neutrality one should substitute $n_i \approx n_e$ into Eq. (3.25). Let n_{e0} be the electron number density arising after the short-term stage of electron production. Taking this value as the initial one and performing integration of this equation we come to the following usual law for binary plasmas

$$n_e = \frac{n_{e0}}{1 + \alpha_d n_{e0} t}. \tag{3.26}$$

Substituting $n_e = n_{e0}/2$ into Eq. (3.26) we obtain the rough estimate of the plasma relaxation time $t_r \sim (\alpha_d n_{e0})^{-1}$. In the altitude range of interest the numerical values of the parameters are as follows: $\alpha_d = (1-3) \times 10^{-7} \, \text{cm}^3 \text{s}^{-1}$ (Lehtinen and Inan 2007) and $n_{e0} = 6 \times 10^4 \, \text{cm}^{-3}$ (Haldoupis et al. 2009). Substituting these values into the above relationship gives the estimate $t_r \sim (2-5) \times 10^2 \, \text{s}$ which is compatible with the recovery time of early VLF events.
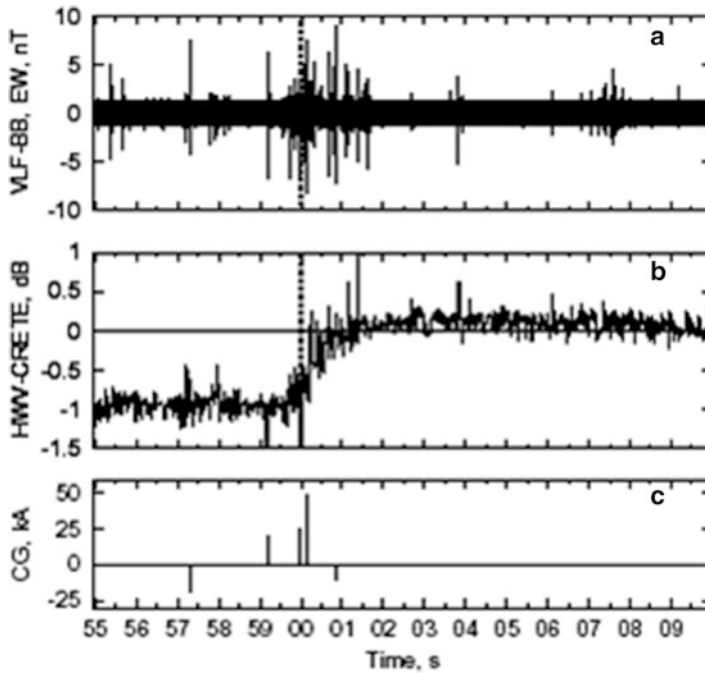
Fig. 3.25 An "early/slow" VLF event (*middle panel b*) which was observed in Crete at the distance about 2,000 km from a convective storm in central France. The sprite appearance was detected at the time marked by the *vertical dashed line*. A signature of the causative $+$CG discharge and other CGs is displayed in the (*bottom panel c*). The sferics possibly associated with intracloud lightning discharges were recorded by a broadband VLF receiver in Nançay, France, at about 200 km northeast of the thunderstorm (*upper panel a*). Adapted from Neubert et al. (2008)

Hence the early VLF events can be associated with the lightning and sprite-produced extra ionization in the D-region. In this picture the recovery time seems to be controlled by the plasma relaxation time.

A new type of the so-called early/slow VLF perturbations associated with sprites have been recently observed (Neubert et al. 2008). An experimental evidence of such events provided by the Crete receiver is shown in Fig. 3.25 (middle panel b). The sprite was observed over a convective storm in central France at the distance about 2,000 km from the receiver. This "early/slow" event is characterized by a relatively long onset time of ~ 2 s after the moment of sprite appearance. As is seen from the bottom panel, this event can be associated with a few sequential CG lightning strokes. The broadband time series (upper panel a) provided by Nançay VLF receiver exhibits a number of sferics possibly associated with bursts of IC lightning discharges. Haldoupis et al. (2006) have assumed that the sequential electromagnetic pulses radiated upwards from horizontal IC discharges accelerate sprite-produced electrons which in turn can result in ionization of the lower ionosphere. One may also speculate that the electron impact upon the ionosphere causes the generation

of secondary electron avalanche thereby ionizing the ionosphere. In this picture the onset of "early/slow" VLF perturbations and the period of sferics clusterization are correlated.

3.2.6 ELF Field Measurements of Sprite-Producing Events

Analysis of the ELF field measurements made it apparent that the sprite-associated events can be accompanied by appearance of two distinct peaks in the ELF recordings (Cummer et al. 1998, 2006a). Simultaneous optical and ELF observations have shown that the first peak corresponds to the causative lightning whereas the second one coincides in time with the moment of sprite luminosity. As is evident from the observations, the currents flowing inside the sprite body may generate 1–2 pulses comparable in amplitude with that produced by a causative CG flash and it appears that the peak amplitude is proportional to the sprite brightness. As one example, Fig. 3.26 shows the ELF field variations caused by +CG causative lightning and sprite which were detected by an interferometric optic system called SAFIR in the Hokuriku area (37.48° N, 136.76° E), Japan on February 03, 2007 during the 2006/2007 winter campaign. The first two peaks in this figure are assumed to be caused by two +CG return strokes while the third peak that follows the first ones can be resulted from the sprite current because this peak practically coincides with the sprite initiation moment (red vertical line in Fig. 3.26) which was found from the optical measurements.

As is seen from Fig. 3.26, the sprite delay between a sprite and its causative +CGs is about 50 ms although the lag time can reach a few hundred ms (Cummer 2003; Cummer et al. 2006a). The same order value seems to be typical as the duration of long-lasting intense CC in the positive causative lightning (Reising et al. 1996; Cummer and Füllekrug 2001; Lyons 2006; Hu et al. 2007). It may be suggested that the CC and possibly the higher frequency components (like M-component) in the CC play an important role in the initiation of the long delayed sprites (Yashunin et al. 2007; Asano et al. 2009a,b). The horizontal lightning currents between clouds and IC lightning discharges followed by nonuniform ionization of the upper atmosphere and an increase in mesospheric electric field can serve as the triggering events for the delayed sprite generation (Bell et al. 1998; Cho and Rycroft 1998, 2001; Ohkubo et al. 2005).

When the ELF recording and luminosity data are compared with that derived from model approximation of the sprite currents, this makes it possible to extract the sprite charge moment change (Boccippio et al. 1995; Hobara et al. 2001, 2006; Cummer 2003; Hayakawa et al. 2004; Matsudo et al. 2009) and also the sprite current moment waveform from the observations (Cummer and Inan 2000). Based on this approach, Cummer et al. (2006a) have estimated the sprite current moments as much as several hundred kA km for two case-studies.

It is notable that the dynamic spectrogram and ULF/ELF power spectrum of sprite-associated events can exhibit an approximately quasi-oscillatory pattern (Surkov et al. 2010). For example, the upper panel in Fig. 3.27 displays the dynamic
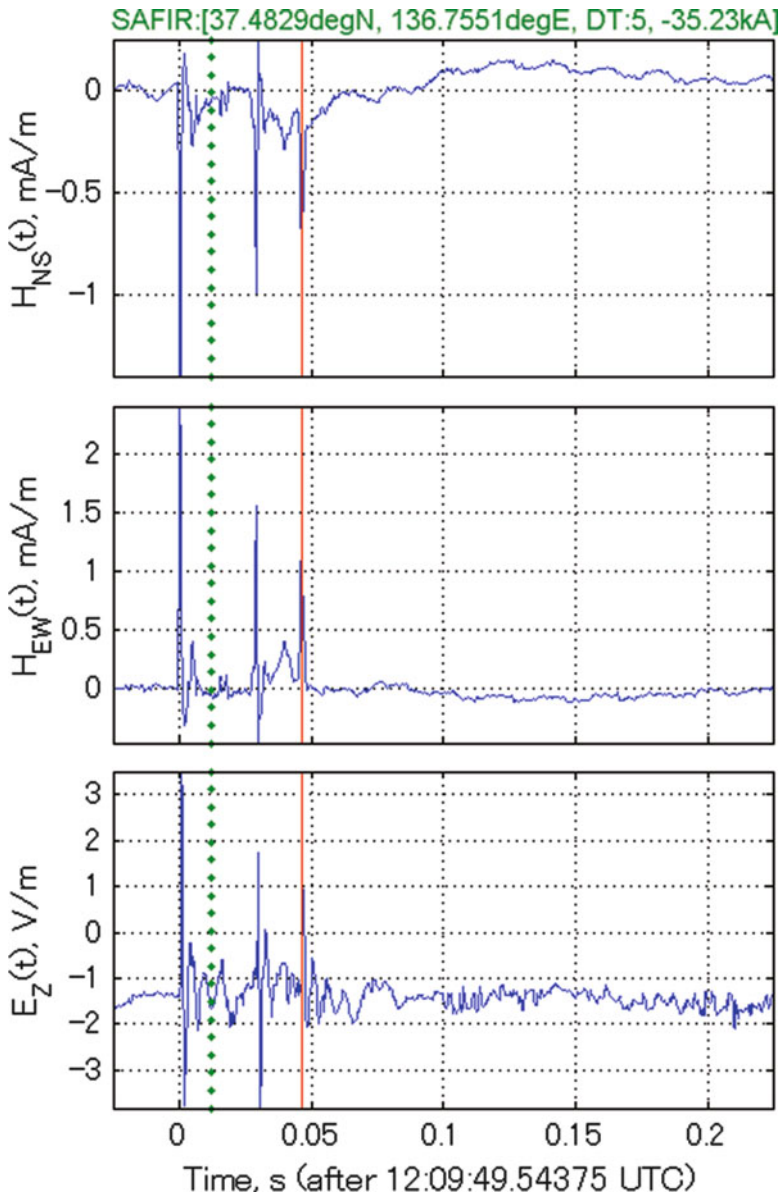
Fig. 3.26 ELF electromagnetic perturbations as observed in the Hokuriku area, Japan (37.48° N, 136.76° E) on February 03, 2007 during a sprite-associated event. The first and middle panels show north-south and east-west, H_{NS} and H_{EW}, magnetic field components while vertical electric field, E_z, is displayed in bottom panel. The vertical *red line* at approximately 0.05 s indicates a moment of sprite flash. Adapted from Surkov et al. (2010)
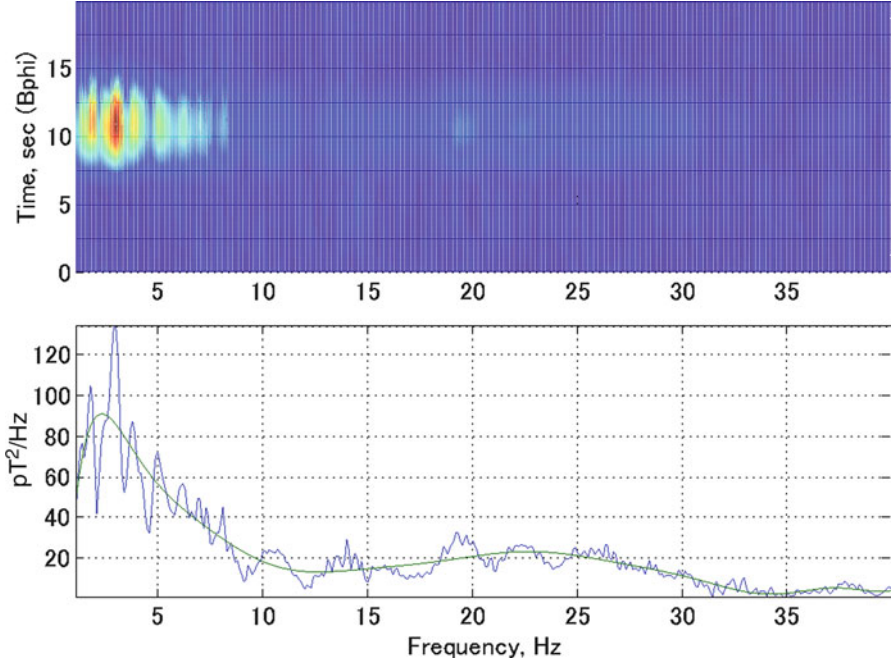
Fig. 3.27 Dynamic spectrogram (*upper panel*) and power spectral density of absolute value of the magnetic field variations shown in Fig. 3.26. Adapted from Surkov et al. (2010)

spectrogram which corresponds to the magnetic variations shown in Fig. 3.26. Every so often the same tendency for oscillating spectra has been observed during the 2006/2007 winter campaign. A distinct resonance structure below 7 Hz is assumed to be due to excitation of the so-called ionospheric Alfvén resonator (IAR) which will be described in more detail in the text section. What is more important, the power spectrum in Fig. 3.27 (lower panel) shows evidence of some vibrations with maximum repetition period of about 15–20 Hz. These oscillations are much more pronounced with the smooth envelope of the power spectrum shown in Fig. 3.27 with green line. To explain this peculiarity, one should note that the spectrum of net magnetic field variations resulted from the causative lightning and the delayed sprite is given by

$$\mathbf{B}(\omega) = \mathbf{B}_c(\mathbf{r}_c, \omega) + \mathbf{B}_s(\mathbf{r}_s, \omega) \exp(i\omega T), \qquad (3.27)$$

where T is the lag of time between the causative lightning and sprite occurrences, and $\mathbf{r}_c$ and $\mathbf{r}_s$ are their position vectors, respectively. Since the power spectrum is proportional to $|\mathbf{B}(\omega)|^2$, it is evident that the amplitude modulation of the power spectrum shown in Fig. 3.27 with green line can be due to the oscillatory factor $\exp(i\omega T)$ in Eq. (3.27). This implies that the sprite lag time is inversely proportional to the "period" $\omega = 2\pi/T$ of spectrum oscillations. In the next section

we shall study a model of the Earth-Ionosphere waveguide which makes it possible to calculate the ULF/ELF spectrum $\mathbf{B}(\omega)$ caused by the lightning discharge and sprite. Comparing the calculated power spectrum with the observation data permits us to find the sprite charge moment, the time lag of the sprite current and other parameters (Surkov et al. 2010). The ULF/ELF measurements thus provide with important information that will assist us in understanding the role played by long-lasting CC and IC processes in the delayed sprite generation.

In conclusion we note that despite much progress toward a comprehension of underlying mechanisms for recently discovered TLEs, the analytical theory of these phenomena is still far from accurate. The numerical modeling continues to be a basic instrument for theoretical study of TLEs behavior except for simple estimates which follow from the similarity law. This approach leaves unexplained why the charge moment change of the causative +CG must be greater than $\sim$500 C km to produce sprites (Stanley et al. 2000; Cummer 2003; Rycroft 2006). Moreover the relationship between the sprite structure and meteorological conditions, the effect of IC lightning activity, and etc. are far from being well understood. There are a lot of such problems to be solved.

References

Allen NL, Ghaffar A (1995) The conditions required for propagation of cathode-directed positive streamer in air. J Phys D Appl Phys 28:331–337

Asano T, Suzuki T, Hiraki Y, Mareev E, Cho MG, Hayakawa M (2009a) Computer simulations on sprite initiation for realistic lightning models with higher-frequency surges. J Geophys Res 114:A02310. doi:10.1029/2008JA013651

Asano T, Suzuki T, Hayakawa M, Cho MG (2009b) Three-dimensional EM computer simulation on sprite initiation above a horizontal lightning discharge. J Atmos Solar Terr Phys 71:983–990

Babaeva NY, Naidis GV (1997) Dynamics of positive and negative streamers in air in weak uniform electric fields. IEEE Trans Plasma Sci 25:375–379

Babich LP, Kutsyk IM, Donskoy EN, Kudryavtsev AY (1998) New data on space and time scales of relativistic runaway electron avalanche for thunderstorm environment: Monte Carlo calculations. Phys Lett A 245:460–470

Babich LP, Kudryavtsev AY, Kudryavtseva ML, Kutsyk IM (2008) Atmospheric gamma-ray and neutron flashes. J Exp Theor Phys 106(1):65–76. doi:10.1007/s11447-008-1005-4

Bazelyan EM, Raizer YP (1998) Spark discharge. CRC Press, Boca Raton

Bell TF, Reising SC, Inan US (1998) Intense continuing currents following positive cloud-cloud lightning associated with red sprites. Geophys Res Lett 25:1285–1288

Berger K, Anderson RB, Kröninger H (1975) Parameters of lightning flashes. Electra 41:23–27

Bering EA III, Few AA, Benbrook JR (1998) The global electric circuit. Phys. Today 51:24–30

Bethe HA (1930) Zur Theorie des Durchgans schneller Korpuskularstrahlen durch Materie. Ann Phys Leipzig B5:325–400

Bhartendu H (1969) Thunder-a survey. Naturaliste Can 96(4):671–682

Bliokh PV, Nickolaenko AP, Filippov YF (1980). In: Llanwyn-Jones D (ed) Schumann resonances in the Earth-ionosphere cavity. Peter Peregrines, London

Boccippio DJ, Williams ER, Heckman SJ, Lyons WA, Baker IT, Boldi R (1995) Sprites, ELF transients, and positive ground strokes. Science 269(5227):1088–1091

Boeck WL, Vaughan OH Jr, Blakeslee R, Vonnegut B, Brook M (1992) Lightning induced brightening in the airglow layer. Geophys Res Lett 19:99–102

Boeck WL, Vaughan OH, Blakeslee RJ, Vonnegut B, Brook M, McKune J (1995) Observations of lightning in the stratosphere. J Geophys Res 100:1465–1475

Bondiou A, Gallimberti I (1994) Theoretical modeling of the development of the positive spark in long gaps. J Phys D Appl Phys 27:1252–1266

Borovsky JE (1998) Lightning energetics: estimates of energy dissipation in channels, channel radii, and channel-heating risetimes. J Geophys Res 103:11537–11553

Bragin YA, Tyutin AA, Kocheev AA, Tyutin AA (1974) Direct measurement of the atmospheric vertical electric field strength up to 80 km. Cosmic Invest [Kosmicheskie Issledovaniya, English Translation] 12:279–280

Briggs MS, Fishman GJ, Connaughton V, Bhat PN, Paciesas WS, Preece RD, Wilson-Hodge C, Chaplin VL, Kippen RM, von Kienlin A, Meegan CA, Bissaldi E, Dwyer JR, Smith DM, Holzworth RH, Grove JE, Chekhtman A (2010) First results on terrestrial gamma ray flashes from the fermi gamma-ray burst monitor. J Geophys Res 115:A00E49. doi:10.1029/2009JA014853

Carlson BE, Lehtinen NG, Inan US (2008) Runaway relativistic electron avalanche seeding in the Earth's atmosphere. J Geophys Res 113:A10307. doi:10.1029/2008JA013210

Carlson BE, Lehtinen NG, Inan US (2010) Terrestrial gamma ray flash production by active lightning leader channels. J Geophys Res 115:A10324. doi:10.1029/2010JA015647

Celestin S, Pasko VP (2010) Effects of spatial non-uniformity of streamer discharges on spectroscopic diagnostics of peak electric fields in transient luminous events. Geophys Res Lett 37:L07804. doi:10.1029/2010GL042675

Celestin S, Pasko VP (2011) Energy and fluxes of thermal runaway electrons produced by exponential growth of streamers during the stepping of lightning leaders and in transient luminous events. J Geophys Res 116:A03315. doi:10.1029/2010JA016260

Chalmers JA (1967) Atmospheric electricity, 2nd edn. Pergamon Press, New York

Chanrion O, Neubert T (2010) Production of runaway electrons by negative streamer discharges. J Geophys Res 115:A00E32

Chen AB, Kuo C-L, Lee Y-J, Su H-T, Hsu R-R, Chern J-L, Frey HU, Mende SB, Takahashi Y, Fukunishi H, Chang Y-S, Liu T-Y, Lee L-C (2008) Global distributions and occurrence rates of transient luminous events. J Geophys Res 113:A08306. doi:10.1029/2008JA013101

Cheng Z, Cummer SA, Su HT, Hsu RR (2007) Broadband very low frequency measurement of D region ionospheric perturbations caused by lightning electromagnetic pulses. J Geophys Res 112:A06318. doi:10.1029/2006JA011840

Chern JL, Hsu RR, Su HT, Mende SB, Fukunishi H, Takahashi Y, Lee LC (2003) Global survey of upper atmospheric transient luminous events on the ROCSAT-2 satellite. J Atmos Solar Terr Phys 65(5):647–659

Cho M, Rycroft MJ (1998) Computer simulation of the electric field structure and optical emission from cloud-top to the ionosphere. J Atmos Solar Terr Phys 60:871–888

Cho M, Rycroft MJ (2001) Non-uniform ionization of the upper atmosphere due to the electromagnetic pulse from a horizontal lightning discharge. J Atmos Solar Terr Phys 63:559–580

Christian HJ, Blakeslee RJ, Boccippio DJ, Boeck WL, Buechler DE, Driscoll KT, Goodman SJ, Hall JM, Koshak WJ, Mach DM, Stewart MF (2003) Global frequency and distribution of lightning as observed from space by the optical transient detector. J Geophys Res 108(D1):4005. doi:10.1029/2002JD002347

Colman JJ, Roussel-Dupré RA, Triplett L (2010). Temporally self-similar electron distribution functions in atmospheric breakdown: the thermal runaway regime. J Geophys Res 115:A00E16. doi:10.1029/2009JA014509

Coroniti SC (1965) Theories of generation in thunderstorm. Problems of atmospheric and space electricity. Elsevier Publishing Co., New York

Cummer SA (2003) Current moment in sprite-producing lightning. J Atmos Solar Terr Phys 65:499–508

Cummer SA, Füllekrug M (2001) Unusually intense CC in lightning produces delayed mesospheric breakdown. Geophys Res Lett 28:495–498

Cummer SA, Inan US, Bell TF, Barrington-Leigh CP (1998) ELF radiation produced by electrical currents in sprites. Geophys Res Lett 25:1281–1284

Cummer SA, Inan US (2000) Modelling ELF radio atmospheric propagation and extracting lightning currents from ELF observations. Radio Sci 35:385–394

Cummer SA, Lyons WA (2005) Implications of lightning charge moment changes for sprite initiation. J Geophys Res 110:A04304. doi: 10.1029/2004JA010812

Cummer SA, Frey HU, Mende SB, Hsu R-R, Su H-T, Chen AB, Fukunishi H, Takahashi Y (2006a) Simultaneous radio and satellite optical measurements of high-altitude sprite current and lightning continuing current. J Geophys Res 111:A10315. doi:10.1029/2006JA011809

Cummer SA, Jaugey N, Li J, Lyons WA, Nelsen TE, Gerken EA (2006b) Submillisecond imaging of sprite development and structure. Geophys Res Lett 33:L04104. doi:10.1029/2005GL024969

Cummer SA, Li J, Han F, Lu G, Jaugey N, Lyons WA, Nelson TE (2009) Quantification of the troposphere-to-ionosphere charge transfer in a gigantic jet. Nature Geosci 2:1–4. doi:10.1038/NGEO607

Derks G, Ebert U, Meulenbroek B (2008) Laplacian instability of planar streamer ionization fronts: an example of pulled front analysis. J Nonlinear Sci 18:551–590

Dowden RL, Brundell JB, Lyons WA, Nelson T (1996) Detection and location of red sprites by VLF scattering of subionospheric transmissions. Geophys Res Lett 23:1737–1740. doi:10.1029/96GL01697

Dwyer J, Smith D, Uman M, Saleh Z, Grefenstette B, Hazelton B, Rassoul H (2010) Estimation of the influence of high-energy electron bursts produced by thunderclouds and the resulting radiation doses received in aircraft. J Geophys Res 115:D09206. doi:10.1029/2009JD012039

Ebert U, Sentman D (2008) Editorial review: streamers, sprites, leaders, lightning: from micro- to macroscales. J Phys D Appl Phys 41:230301

Ebert U, Nijdam S, Li C, Luque A, Briels T, van Veldhuizen E (2010) Review of recent results on streamer discharges and discussion of their relevance for sprites and lightning. J Geophys Res 115:A00E43. doi:10.1029/2009JA014867

Fernsler R, Rowland H (1996) Models of lightning-produced sprites and elves. J Geophys Res 101:29653–29662

Feynman RP, Leighton RB, Sands M (1964) The Feynman lectures on physics, vol 2. Addison-Wesley/Readings: Palo Alto/London

Fishman GJ, Bhat PN, Mallozzi R, Horack JM, Koshut T, Kouveliotou C, Pendleton GN, Meegan CA, Wilson RB, Paciesas WS, Goodman SJ, Christian HJ (1994) Discovery of intense gamma-ray flashes of atmospheric origin. Science 264:1313–1316

Franz RC, Nemzak RJ, Winkler JR (1990) Television image of a large upward electrical discharge above a thunderstorm system. Science 249:48–51

Fukunishi H, Takahashi Y, Fujito M, Wanatabe Y, Sakanoi S (1996) Fast imagining of elves and sprites using a framing/streak camera and a multi-anode array photometer. EOS Trans AGU 77(46, Fall Meeting Suppl.):F60

Füllekrug M, Constable S (2000) Global triangulation of intense lightning discharges. Geophys Res Lett 27(3):333–336

Füllekrug M, Fraser-Smith AC, Bering EA, Few AA (1999) On the hourly contribution of global cloud-to-ground lightning activity to the atmospheric electric field in the Antarctic during December 1992. J Atmos Solar Terr Phys 61:745–750

Füllekrug M, Roussel-Dupré RA, Symbalisty EMD, Chanrion O, Odzimek A, van der Velde O, Neubert T (2010) Relativistic runaway breakdown in low-frequency radio. J Geophys Res 115:A00E09. doi:10.1029/2009JA014468

Füllekrug M, Roussel-Dupré R, Symbalisty EMD, Colman JJ, Chanrion O, Soula S, van der Velde O, Odzimek A, Bennett AJ, Pasko VP, Neubert T (2011) Relativistic electron beams above thunderclouds. Atmos Chem Phys 11:7747–7754

Gerken EA, Inan US, Barrington-Leigh CP (2000) Telescopic imaging of sprites. Geophys Res Lett 27(17):2637–2640

Glukhov V, Pasko V, Inan U (1992) Relaxation of transient lower ionospheric disturbances caused by lightning-whistler-induced electron precipitation bursts. J Geophys Res 97:16971–16979

Gurevich AV, Milikh GM, Roussel-Dupré R (1992) Runaway electron mechanism of air breakdown and preconditioning during a thunderstorm. Phys Lett A 165:463–468

Gurevich AV, Milikh GM, Roussel-Dupré R (1994) Nonuniform runaway air-breakdown. Phys Lett A 187:197–203

Gurevich AV, Zybin KP (2001) Runaway breakdown and electric discharges in thunderstorm. Phys. Uspekhi 44:1119–1140

Gurevich AV, Zybin KP (2004) High energy cosmic ray particles and the most powerful discharges in thunderstorm atmosphere. Phys Lett A 329:341–347. doi:10.1016/j.physleta.2004.06.094

Gurevich AV, Zybin KP, Roussel-Dupré RA (1999) Lightning initiation by simultaneous effect of runway breakdown and cosmic ray shower. Phys Lett A 254:79–97

Gurevich A, Zybin K, Medvedev Y (2007) Runaway breakdown in strong electric field as a source of terrestrial gamma flashes and gamma bursts in lightning leader steps. Phys Lett A361:119–125

Haldoupis C, Steiner RJ, Mika Á, Shalimov S, Marshall RA, Inan US, Bösinger T, Neubert T (2006) "Early/slow" events: a new category of VLF perturbations observed in relation with sprites. J Geophys Res 111:A11321. doi:10.1029/2006JA011960

Haldoupis C, Mika Á, Shalimov S (2009) Modeling the relaxation of early VLF perturbations associated with transient luminous events. J Geophys Res 114:A00E04. doi:10.1029/2009JA014313

Hale LC, Croskey CL, Mitchell JD (1981) Measurements of middle-atmosphere electric fields and associated electrical conductivities. Geophys Res Lett 8:927–930

Hayakawa M, Nakamura T, Hobara Y, Williams E (2004) Observation of sprites over the sea of Japan and conditions for lightning-induced sprites in winter. J Geophys Res 105:4689–4697

Hayakawa M, Sekiguchi M, Nickolaenko AP (2005) Diurnal variations of electric activity of global thunderstorms deduced from OTD data. J Atmos Electr 25(2):55–68

Hayakawa M, Hobara Y, Suzuki T (2012) Lightning effects in the mesosphere and ionosphere. In: Cooray V (ed) Lightning electromagnetics. Institution of Engineering and Technology, London, pp 611–646

Heavner MJ, Sentman DD, Moudry DR, Wescott EM (2000) Sprites, blue jets, and elves: optical evidence of energy transport across the stratopause. In: Siskind DE, Eckermann SD, Summers ME (eds) Atmospheric science across the stratosphere. Geophysical monograph series, vol 123. AGU, Washington, DC, pp 69–82

Heavner MJ, Suszcynsky DM, Smith DA (2003) LF/VLF intracloud waveform classification. Paper presented at International Conference on Atmospheric Electricity, ICAE, Versailes, France

Helliwell R, Katsufrakis JP, Trimpi M (1973) Whistler-induced amplitude perturbation in VLF propagation. J Geophys Res 78:4679–4688

Hiraki Y, Fukunishi H (2007) Theoretical criterion of charge moment change by lightning for initiation of sprites. J Geophys Res 111:A11305

Hobara Y, Iwasaki N, Hayashida T, Hayakawa M, Ohta K, Fukunishi H (2001) Interrelation between ELF transients and ionospheric disturbances in association with sprites and elves. Geophys Res Lett 28:935–938

Hobara Y, Hayakawa M, Williams E, Boldi R, Downes E (2006) Location and electrical properties of sprite-producing lightning from a single ELF site. In: Füllekrug M, Mareev EA, Rycroft MJ (eds) Sprites, elves and intense lightning discharges. NATO science series II, vol 225. Springer, Dordrecht, pp 211–235

Hu W, Cummer SA, Lyons WA (2007) Testing sprite initiation theory using lightning measurements and modeled EM fields. J Geophys Res 112:D13115

Imyanitov IM, Chubarina EV, Schwartz YM (1971) Electricity of clouds. Gydrometeoizdat, Leningrad, p 239 (in Russian)

Inan US, Lehtinen NG (2005) Production of terrestrial gammaray flashes by an electromagnetic pulse from a lightning return stroke. Geophys Res Lett 32:L19818. doi:10.1029/2005GL023702

Inan US, Bell TF, Pasko VP, Sentman DD, Wescott EM, Lyons WA (1995) VLF signatures of ionospheric disturbances associated with sprites. Geophys Res Lett 22:3461–3464. doi:10.1029/95GL03507

Inan US, Sampson WA, Taranenko YN (1996a) Space-time structure of optical flashes and ionization changes produced by lightning-EMP. Geophys Res Lett 23:133–136. doi:10.1029/95GL03816

Inan US, Reising SC, Fishman GJ, Horack JM (1996b) On the association of terrestrial gamma-ray bursts with lightning and implications for sprites. Geophys Res Lett 23:1017–1020

Inan US, Barrington-Leigh C, Hansen S, Glukhov VS, Bell TF, Rairden R (1997) Rapid lateral expansion of optical luminosity in lightning-induced ionospheric flashes referred to as "elves" . Geophys Res Lett 24(5):583–586

Inan US, Cummer SA, Marshall RA (2010) A survey of ELF and VLF research on lightning-ionosphere interactions and causative discharges, J Geophys Res 115, A00E36. doi:10.1029/2009JA014775

Ishikawa H (1961) Nature of lightning discharge as origin of atmospherics. Proc. Res. Inst. Atmos Nagoya Univ 8A:1–274

Israël H (1970) Atmospheric electricity, vol 1, 2nd edn. Israel Program for Scientific Translations, Jerusalem

Israël H (1973) Atmospheric electricity, vol 2, 2nd edn. Israel Program for Scientific Translations, Jerusalem

Jacobson AR (2003) Relationship of intracloud lightning radiofrequency power to lightning storm height, as observed by the FORTE satellite. J Geophys Res 108(D7):4204. doi:10.1029/2002JD002956

Jones DLl (1970) Electromagnetic radiation from multiple return stroke of lightning. J Atmos Terr Phys 32:1077–1093

Krehbiel PR, Riousset JA, Pasko VP, Thomas RJ, Rison W, Stanley MA, Edens HE (2008) Upward electrical discharges from thunderstorms. Nature Geosci 1(4):233–237. doi:10.1038/ngeo162

Krider EP (1986) Physics of lightning. In: Earth's electrical environment. National Academy Press, Washington, DC, pp 30–40

Kudintseva IG, Nickolaenko AP, Hayakawa M (2009) Spatial fine structure of model electric pulses in mesosphere above Γ -shaped stroke of lightning. Surv Geophys 71:603–608

Kudintseva IG, Nickolaenko AP, Hayakawa M (2010) Transient electric field in the mesosphere above a Γ-shape lightning stroke. Surv Geophys 31:427–448. doi:10.1007/s10712-0010-9095-x

Kuo C, Chou JK, Tsai LY, Chen AB, Su HT, Hsu RR, Cummer SA, Frey HU, Mende SB, Takahashi Y, Lee LC (2009) Discharge process, electric field, and electron energy in ISUAL-recorded gigantic jets. J Geophys Res 114:A04314. doi:10.1029/2008JA013791

Lehtinen N (2000) Relativistic runaway electrons above thunderstorms. Ph.D. dissertation, Stanford University

Lehtinen NG, Inan US (2007) Possible persistent ionization caused by giant blue jets. Geophys Res Lett 34:L08804. doi:10.1029/2006GL029051

Lehtinen N, Bell T, Pasko V, Inan U (1997) A two-dimensional model of runaway electron beams driven by quasi-electrostatic thundercloud fields. Geophys Res Lett 24:2639–2642

Lehtinen N, Bell T, Inan U (1999) Monte Carlo simulation of runaway MeV electron breakdown with application to red sprites and terrestrial gamma ray flashes. J Geophys Res 104:24699–24712

Li C, Ebert U, Hundsdorfer W (2009) 3D hybrid computations for streamer discharges and production of run-away electrons. J Phys D Appl Phys 42:202003

Li C, Ebert U, Hundsdorfer W (2010) Spatially hybrid computations for streamer discharges with generic features of pulled fronts: I. Planar fronts. J Comput Phys 229:200

Lieberman MA, Lichtenberg AJ (1994) Principles of plasma discharges and material processing. Wiley, New York

Liu NY, Pasko VP (2006) Effects of photoionization on similarity properties of streamers at various pressures in air. J Phys D Appl Phys 39:327–334. doi:10.1088/0022-3727/39/2/013

Luque A, Ebert U (2009) Emergence of sprite streamers from screening-ionization waves in the lower ionosphere. Nature Geosci 2:757–760. doi:10.1038/ngeo662

Luque A, Ebert U (2010) Sprites in varying air density: charge conservation, glowing negative trails and changing velocity. Geophys Res Lett 37:L06806. doi:10.1029/2009GL041982

Luque A, Ebert U (2012) Density models for streamer discharges: beyond cylindrical symmetry and homogeneous media. J Comput Phys 231:904–918. doi:10.1016/j.jcp.2011.04.019

Lyons WA (1997) The handy weather answer book. Accord Publishing, Detroit

Lyons WA (2006) The meteorology of transient luminous events. An introduction and overview. In: Füllekrug M, Mareev EA, Rycroft MJ (eds) Sprites, elves and intense lightning discharges. NATO Science Series II, vol 225. Springer, Dordrecht, pp 19–44

Lyons WA, Nelson T, Williams ER, Cummer SA, Stanley MA (2003) Characteristics of sprite-producing positive cloud-to-ground lightning during the 19 July STEPS mesoscale convective systems. Mon Weather Rev 131:2417–2427

Mareev EA, Trakhtengerts VY (2007) Puzzles of atmospheric electricity. Priroda 3:24–33 (in Russian)

Marshall T, McCarthy MP, Rust WD (1995) Electric field magnitudes and lightning initiation in thunderstorms. J Geophys Res 100(D4):7097–7103. doi:10.1029/95JD00020

Matsudo Y, Suzuki T, Hayakawa M, Yamashita K, Ando Y, Michimoto K, Korepanov V (2007) Characteristics of Japanese winter sprites and their parent lightning as estimated by VHF lightning and ELF transients. J Atmos Solar Terr Phys 69:1431–1446

Matsudo Y, Suzuki T, Michimoto K, Myokei K, Hayakawa M (2009) Comparison of time delays of sprites induced by winter lightning flashes in the Japan Sea with those in the Pacific Ocean. J Atmos Solar Terr Phys 71:101–111

Maynard NC, Croskey CL, Mitchell JD, Hale LC (1981) Measurement of volt/meter vertical electric fields in the middle atmosphere. Geophys Res Lett 8:923–926

McGorman DR, Rust WD (1998) The electrical nature of storms. Oxford University Press, Oxford, p 422

McHarg MG, Stenbaek-Nielsen HC, Kanmae T (2007) Observation of streamer formation in sprites. Geophys Res Lett 34:L06804. doi:10.1029/2006GL027854

Mende, SB, Frey HU, Hsu RR, Su HT, Chen AB, Lee LC, Sentman DD, Takahashi Y, Fukunishi H (2005) D region ionization by lightning-induced electromagnetic pulses. J Geophys Res 110:11312. doi:10.1029/2005JA011064

Milikh G, Roussel-Dupré R (2010) Runaway breakdown and electrical discharges in thunderstorms. J Geophys Res 115:A00E60. doi:10.1029/2009JA014818

Mishin EV, Milikh GM (2008) Blue jets: upward lightning. Space Sci Rev 137(1–4):473–488

Montanyà J, van der Velde O, Romero D, March V, Solá G, Pineda N, Arrayas M, Trueba JL, Reglero V, Soula S (2010) High-speed intensified video recordings of sprites and elves over the western Mediterranean Sea during winter thunderstorms. J Geophys Res 115:A00E18. doi:10.1029/2009JA014508

Muchnik VM, Fishman BE (1982) Electrization of coarse-dispersion aerosols in the atmosphere. Gidrometeoizdat, Leningrad (in Russian)

Myokei K, Matsudo Y, Asano T, Suzuki T, Hobara Y, Michimoto K, Hayakawa M (2009) A study of the morphology of winter sprites in the Hokuriku area of Japan in relation to cloud height. J Atmos Solar Terr Phys 71:579–602

Nelson PH (1967) Ionospheric perturbations and Schumann resonances data. Ph.D. thesis, MIT, Cambridge

Neubert T, Allin TH, Blanc E, Farges T, Haldoupis C, Mika A, Soula S, Knutsson L, van der Velde O, Marshall RA, Inan U, Sátori G, Bór J, Hughes A, Collier A, Laursen S, Rasmussen IL (2005) Co-ordinated observations of transient luminous events during the Eurosprite2003 campaign. J Atmos Solar Terr Phys 67:807–820. doi:10.1016/j.jastp.2005.02.004

Neubert T, Rycroft M, Farges T, Blanc E, Chanrion O, Arnone E, Odzimek A, Arnold N, Enell C-F, Turunen E, Bösinger T, Mika Á, Haldoupis C, Steiner RJ, van der Velde O, Soula S, Berg P, Boberg F, Thejll T, Cristiansen B, Ignaccolo M, Füllekrug M, Verronen PT, Montanyá J,

Crosby N (2008) Recent results from studies of electric discharges in the mesosphere. Surv Geophys 29:71–137. doi:10.1007/s10712-008-9043-1

Neubert T, Chanrion O, Arnone E, Zanotti F, Cummer S, Li J, Füllekrug M, Soula S, van der Velde O (2011) The properties of a gigantic jet reflected in a simultaneous sprite: observations interpreted by a model. J Geophys Res 116:A12329. doi:10.1029/2011JA016928

Nickolaenko AP, Hayakawa M (1995) Heating of the lower ionosphere electrons by electromagnetic radiation of lightning discharges. Geophys Res Lett 22:3015–3018

Nickolaenko AP, Hayakawa M (1998) Electric fields produced by lightning discharges. J Geophys Res 103:17175–17189

Nickolaenko AP, Hayakawa M (1999) A model for causative discharge of ELF-transients. J Atmos Electr 19:11–24

Nickolaenko AP, Hayakawa M (2002) Resonances in the earth-ionosphere cavity. Kluwer Academic Publishers, Dordrecht, p 380

Nickolaenko AP, Hayakawa M (2014) Schumann resonances for tyros. Springer, Tokyo, p 348

Ogawa T (1995) Lightning currents. In: Volland H (ed) Handbook of atmospheric electrodynamics, 1. CRC Press, Florida, pp 93–136

Ohkubo A, Fukunishi H, Takahashi Y, Adachi T (2005) VLF/ELF sferic evidence for in-cloud discharge activity producing sprites. Geophys Res Lett 32:L04812. doi:10.1029/2004GL021943

Otsuyama T, Manaba J, Hayakawa M, Nishimura M (2004) Characteristics of subionospheric VLF perturbation associated with winter lightning around Japan. Geophys Res Lett 31:L04117. doi:10.1029/2003GL019064

Paiva GS, Pavão AC, Bastos CC (2009) "Seed" electrons from muon decay for runaway mechanism in the terrestrial gamma ray flash production. J Geophys Res 114:D03205. doi:10.1029/2008JD010468

Pancheshnyi S (2005) Role of electronegative gas admixtures in streamer start, propagation and branching phenomena. Plasma Sources Sci Technol 14:645–653

Pasko VP (2006) Theoretical modeling of sprites and jets. In: Füllekrug M, Mareev EA, Rycroft MJ (eds) Sprites, elves and intense lightning discharges. NATO Science Series II, vol 225. Springer, Dordrecht, pp 255–311

Pasko VP (2010) Recent advances in theory of transient luminous events. J Geophys Res 115:A00E35. doi:10.1029/2009JA014860

Pasko VP, Inan US, Bell TF (2000) Fractal structure of sprites. Geophys Res Lett 27:497–500

Pasko VP, Inan US, Bell TF (2001) Mesosphere-ionosphere coupling due to sprites. Geophys Res Lett 28:3821–3824

Pasko VP, Stanley MA, Matheus JD, Inan US, Wood TG (2002) Electrical discharge from a thunderstorm top to the lower ionosphere. Nature 416:152–154

Pasko VP, Qin J, Celestin S (2013) Toward better understanding of sprite streamers: initiation, morphology, and polarity asymmetry. Surv Geophys 34(6):797–830. doi:10.1007/s10712-013-9246-y

Petrov NI, Petrova GN (1999) Physical mechanism for the development of lightning discharges between a thundercloud and the ionosphere. Tech Phys 44:472–475

Raizer YP (1991) Gas discharge physics. Springer, Berlin

Raizer YP, Milikh GM, Shneider MN, Novakovski SV (1998) Long streamer in the upper atmosphere above thundercloud. J Phys D Appl Phys 31:3255–3264

Raizer YP, Milikh GM, Shneider MN (2006) On the mechanism of blue jet formation and propagation. Geophys Res Lett 33(23):L23801. doi:10.1029/2006GL027697

Raizer YP, Milikh GM, Shneider MN (2007) Leader-streamers nature of blue jets. J Atmos Solar Terr Phys 69(8):925–938. doi:10.1016/j.jastp.2007.02.007

Raizer YP, Milikh GM, Shneider MN (2010) Streamer-and leader-like processes in the upper atmosphere: models of red sprites and blue jets. J Geophys Res 115:A00E42. doi:10.1029/2009JA014645

Rakov VA (2000) Positive and bipolar lightning discharges: a review. In: Proceedings of the 25th International Conference on Lightning Protection, Rhodos, pp 103–108

Rakov VA (2003) A review of positive and bipolar lightning discharges. Bull Am Meteorol Soc 84:767–775

Rakov VA, Uman MA (1998) Review and evaluation of lightning return stroke models including some aspect of their application. IEEE Trans Electromagn Compatibility 40:403–426

Rakov VA, Uman MA (2003) Lightning: physics and effects. Cambridge University Press, Cambridge, p 687

Reising SC, Inan US, Bell TF, Lyons WA (1996) Evidence for CCs in sprite-producing cloud-to-ground lightning. Geophys Res Lett 23:3639–3642

Riousset JA, Pasko WA, Krehbiel PR, Rison W, Stanley MA (2010a) Modeling of thundercloud screening charges: implications for blue and gigantic jets. J Geophys Res 115:A00E10. doi:10.1029/2009JA014286

Riousset JA, Pasko VP, Bourdon A (2010b) Air-density-dependent model for analysis of air heating associated with streamers, leaders, and transient luminous events. J Geophys Res 115:A12321. 10.1029/2010JA015918

Roussel-Dupré R, Gurevich A (1996) On runaway breakdown and upward propagating discharges. J Geophys Res 101:2297–2311

Roussel-Dupré R, Colman JJ, Symbalisty E, Sentman D, Pasko VP (2008) Physical processes related to discharges in planetary atmospheres. Space Sci Rev 137:51–82. doi:10.1007/s11214-008-9385-5

Rowland HL (1998) Theories and simulations of elves, sprites and blue jets. J Atmos Solar Terr Phys 60:831–844

Rycroft MJ (2006) Introduction to the physics of sprites, elves and intense lightning discharges. In: Füllekrug M, Mareev EA, Rycroft MJ (eds) Sprites, elves and intense lightning discharges. NATO Science Series II, vol 225. Springer, Dordrecht, pp 1–18

Rycroft MJ, Israelsson S, Price C (2000) The global atmospheric electric circuit, solar activity and climate change. J Atmos Solar Terr Phys 62:1563–1576

Sato M, Fukunishi H (2003) Global sprite occurrence locations and rates derived from triangulation of transient Schumann resonances events. Geophys Res Lett 30(16):1859. doi:10.1029/2003GL017291

Sato M, Takahashi Y, Yoshida A, Adachi T (2008) Global distribution of intense lightning discharges and their seasonal variations. J Phys D Appl Phys 41:234011. doi:10.1088/0022-3727/41/23/234011

Sátori G, Williams E, Lemperger I (2009) Variability of global lightning activity on the ENSO time scale. Atmos Res 91:500–507

Schonland BEJ (1956) The lightning discharge. In: Handbuch der physik, Bd22. Springer, Berlin

Sentman DD, Wescott EM (1993) Observations of upper atmosphere optical flashes recorded from an aircraft. Geophys Res Lett 20:2857–2860

Sentman DD, Wescott EM, Osborne DL, Hampton DL, Heavner MJ (1995) Preliminary results from the Sprites94 aircraft campaign: 1. Red sprites. Geophys Res Lett 22:1205–1208

Smith DA, Shao XM, Holden DN, Rhodes CT, Brook M, Krehbiel PR, Stanley M, Rison W, Thomas RJ (1999) A distinct class of isolated intracloud lightning discharges and their associated radio emissions. J Geophys Res 104:4189–4212

Smith DA, Heavner MJ, Jacobson AR, Shao XM, Massey RS, Sheldon RJ, Wines KC (2004) A method for determining intracloud lightning and ionospheric heights from VLF/LF electric field records. Radio Sci. 39:RS1010. doi:10.1029/2002RS002790

Smith DM, Lopez LI, Lin LI, Barrington-Leigh LI (2005) Terrestrial gamma-ray flashes observed up to 20 MeV. Science 307:1085–1088

Smith DM, Hazelton BJ, Grefenstette BW, Dwyer BW, Holzworth RH, Lay EH (2010) Terrestrial gamma ray flashes correlated to storm phase and tropopause height. J Geophys Res 115:A00E49. doi:10.1029/2009JA014853

Soloviev SP, Surkov VV (2000) Electrostatic field and lightning generated in the gaseous dust cloud of explosive products. Geomagn Aeron 40:61–69

Stanley M, Krehbiel P, Brook M, Moore C, Rison W, Abrahams B (1999) High speed video of initial sprite development. Geophys Res Lett 26:3201–3204

Stanley M, Brook M, Krehbiel P, Cummer S (2000) Detection of daytime sprites via a unique sprite ELF signature. Geophys Res Lett 27:871–874

Stekolnikov IS (1940) Lightning. USSR Academy of Science, Leningrad (in Russian)

Stenbaek-Nielsen HC, Moudry DR, Wescott EM, Sentman DD, Sao Sabbas FT (2000) Sprites and possible mesospheric effects. Geophys Res Lett 27:3829–3832

Stenbaek-Nielsen HC, McHarg MG, Kanmae T, Sentman DD (2007) Observed emission rates in sprite streamer heads. Geophys Res Lett 34:L11105. doi:10.1029/2007GL029881

Stenbaek-Nielsen HC, McHarg MG (2008) High time-resolution sprite imagining: observation and implications. J Phys D Appl Phys 41:234009

Su HT, Hsu RR, Chen RR, Wang YC, Hsiao WS, Lai WC, Lee LC, Sato M, Fukunishi H (2003) Gigantic jets between a thundercloud and the ionosphere. Nature 423:974–976

Surkov VV, Hayakawa M (2012) Underlying mechanisms of transient luminous events: a review. Ann Geophys 30:1185–2012. doi:10.5194/angeo-30-1185-2012

Surkov VV, Matsudo Y, Hayakawa M, Goncharov SV (2010) Estimation of lightning and sprite parameters based on observation of sprite-producing lightning power spectra. J Atmos Solar Terr Phys 72:448–456

Suzuki T, Matsudo Y, Asano T, Hayakawa M, Michimoto K (2011) Meteorological and electrical aspects of several winter thunderstorms with sprites in the Hokuriku area of Japan. J Geophys Res 116:D06205. doi:10.1029/2009JD013358

Taylor WL (1972) Atmospherics and severe storms. In: Deer VE (ed) Remote sensing of the troposphere. Chapter 17, US Government Printing Office, Washington, DC

Trakhtengerts VY, Rycroft MJ (2008) Whistler and Alfvén Mode Cyclotron Masers in Plasma. Cambridge University Press, Cambridge, p 354

Trakhtengerts VY, Iudin DI, Kulchitsky AV, Hayakawa M (2002) Kinetics of runaway electrons in a stochastic electric field. Phys Plasmas 9:2762–2766

Trakhtengerts VY, Iudin DI, Kulchitsky AV, Hayakawa M (2003) Electron acceleration by a stochastic electric field on the atmospheric layer. Phys Plasmas 10:3290–3296

Vallance-Jones A (1974) Aurora. D. Reidel, Dordrecht

van der Velde OA, Mika A, Soula S, Haldoupis C, Neubert T, Inan US (2006) Observations of the relationship between sprite morphology and in-cloud lightning processes. J Geophys Res 111:D15203. doi:10.1029/2005JD006879

van der Velde OA, Lyons WA, Nelson TE, Cummer SA, Li J, Bunnell J (2007) Analysis of the first gigantic jet recorded over continental North America. J Geophys Res 112:D20104. doi:10.1029/2007JD008575

van der Velde OA, Bór J, Li J, Cummer SA, Arnone E, Zanotti F, Füllekrug M, Haldoupis C, NaitAmor S, Farges T (2010) Multi-instrumental observations of a positive gigantic jet produced by a winter thunderstorm in Europe. J Geophys Res 115:D24301. doi:10.1029/2010JD014442

Visacro S, Soares A Jr, Schroeder MAO, Cherchiglia LCL, de Sousa VJ (2004) Statistical analysis of lightning current parameters: measurements at Morro do Cachimbo Station. J Geophys Res 109:D01105. doi: 10.1029/2003JD003662

Uman MA (1987) The lightning discharge. Academic Press, New York

Uman MA, Krider EP (1982) A review of natural lightnings: experimental data and modeling. IEEE Trans Electromagn Compatibility 24:79

Wahlin L (1973) A possible origin of atmospheric electricity. Found Phys 3:450–472

Watt AD (1967) VLF radio engineering. Pergamon Press, New York

Wescott EM, Sentman D, Osborne D, Hampton D, Heavner M (1995) Preliminary results from the Sprites94 aircraft campaign: 2. Blue jets. Geophys Res Lett 22:209–1212

Wescott EM, Sentman DD, Heavner MJ, Hampton DL, Osborne DL, Vaugham OH Jr (1996) Blue starters: brief upward discharges from an intense Arkansas thunderstorm. Geophys Res Lett 23:2153–2156

Wescott EM, Sentman DD, Heavner MJ, Hampton DL, Lyons WA, Nelson T (1998) Observations of columniform sprites. J Atmos Solar Terr Phys 60:733–740

Wescott EM, Sentman DD, Stenbaek-Nielsen HC, Huet P, Heavner MJ, Moudry DR (2001) New evidence for the brightness and ionization of blue starters and blue jets. J Geophys Res 106:21549–21554

Williams E, Downes E, Boldi R, Lyons W, Heckman S (2007) Polarity asymmetry of sprite-producing lightning: a paradox? Radio Sci 42:RS2S17. doi:10.1029/2006RS003488

Wilson CTR (1925) The electric field of a thundercloud and some of its effects. Proc Phys Soc London 37:32D–37D

Winn WP, Schwede GW, Moore CB (1974) Measurements of electrical fields in thunderclouds. J Geophys Res 79(12):1761–1767

Yair Y, Israelevich P, Devir AD, Moalem M, Price C, Joseph JH, Levin Z, Ziv B, Sternlieb A, Teller A (2004) New observations of sprites from space shuttle. J Geophys Res 109:D15201. doi:10.1029/2003JD004497

Yashunin SA, Mareev EA, Rakov VA (2007) Are lightning M components capable of initiating sprites and sprite halo? J Geophys Res 112:D10109. doi:10.1029/2006JD007631

Yukhimuk V, Roussel-Dupré R, Symbalisty EMD (1999) On the temporal evolution of red sprites: runaway theory versus data. Geophys Res Lett 26:679–682